FM0802

THE LARGE APERTURE SEISMIC EXPERIMENT

PART I: DATA ACQUISITION AND ANALYSIS

by

the LASE Study Group

April 29, 1983

Preprint

TABLE OF CONTENTS

PAGE

ABSTRACT

The developing interest in tectonic processes at passive rifted continental margins has created a need for improved knowledge of their deep geological structure, particularly in the region of the transition from oceanic to continental crust. LASE (Large Aperture Seismic Experiment) was a multi-ship, multi-institutional experiment carried out in 1981 to test and evaluate new seismic techniques for investigating the deep structure of continental margins. Using multiple shooting and receiving ships, a 13-km Common Depth Point (CDP) aperture was synthesized with the object of improving the detection and resolution of deep reflectors. In addition, nine expanding spread profiles (ESPs), in which both reflected and refracted seismic energy are observed, were shot with airgun and explosive sources. We describe here the experimental techniques and analysis methods used and the seismic results. Principal among the latter is the observation of a deep 7.2 km/sec reflection event that extends across the margin and a detailed definition of the velocity structure under the prograding carbonate sequence.

I. INTRODUCTION

The LASE experiment was conducted across the Baltimore Canyon Trough, a region of the eastern U.S. margin where many other geological and geophysical investigations have been focused (Figure 1). These include stratigraphic studies using the COST B2 well drilled on the outer shelf and the COST B3 well on the slope (Scholle, 1977; 1980). These data and conventional multi-channel seismic data have heretofore provided the basis for the description of the regional stratigraphy and structure of the sedimentary basin occupying the margin (Grow et al., 1979a; Schlee, 1981). These studies suggest that the basin contains about 14 km of sediments beneath the outer shelf and slope, which may include sediments as old as Triassic. However, the great depth of sediment effectively masks the basement structure, and the COST wells penetrated only Upper Jurassic and younger sediments. The subsidence history of the region has been described by Steckler and Watts (1978); Watts and Steckler (1979); and Sawyer et al. (1982), but these studies were limited by the lack of information on the deep structure of the margin.

Previously, the deep structure inferred from seismic refraction and gravity data (Sheridan et al., 1979; Grow et al., 1979b) gave no estimate of the depth to the crust-mantle

boundary, except over oceanic crust seaward of the transition region. Gravity data have provided estimates of the deep structure in the vicinity of the ocean-continent transition, but these estimates are poorly constrained. The East Coast Magnetic Anomaly, which trends sub-parallel to the edge of the shelf and extends from the Blake Plateau to Nova Scotia [Klitgord and Schouten (in preparation); Klitgord and Behrendt, 1979] lies over the shelf in this region. It exhibits amplitudes of 200 to 300 nT. Its position, which is thought to mark the ocean-continent transition, suggests that the transition occurs landward of the present edge of the shelf, beneath the deepest part of the sedimentary basin. The cause of the magnetic anomaly is unclear, although it forms a prominent marker along the margin.

The uncertainties in the nature of the deep structure of the margin prevent a complete understanding of the processes involved in the evolution of this and other regions of the rifted margin off eastern North America. In an attempt to derive new information about the deep structure of this continental margin, Lamont-Doherty Geological Observatory (L-DGO) of Columbia University, the University of Texas Marine Science Institute (UTMSI), the Woods Hole Oceanographic Institution (WHOI) and Bedford Institute of Oceanography (BIO), carried out a series of multi-channel seismic lines, using three ships to acquire large synthetic aperture profiles.

The first profiles were CDP lines (Figure 1), designed to continuously obtain reflection information from the deepest sedimentary strata, basement and intrabasement horizons, using a 13-km synthetic aperture. This aperture was formed by arranging three ships in line and at predetermined constant offsets. By alternately firing their source arrays and recording all offset combinations, the physical array lengths were magnified and a large synthetic aperture was formed (Buhl et al., 1982).

The second profiling method was designed to obtain precise velocity information for these deep strata at critical locations along the large aperture CDP lines by using two ships in the expanding spread seismic reflection/refraction method (Stoffa and Buhl, 1979).

In this paper we describe the seismic acquisition and analysis methods used to derive information on the deep structure of the Baltimore Canyon Trough and ocean to continent transition. In Part II, we describe in detail the geological implications of these results.

II. DATA ACQUISITION

1. LASE CDP Profiling

A large synthetic aperture receiving array was deployed in order to focus energy from reflection interfaces at great depth within and beneath the thick sedimentary accumulations on the east coast continental margin. Conventional 2.4-3.6 km arrays do not provide sufficient normal moveout to give accurate array velocity information and often they do not receive sufficient reflection energy to produce continuous seismic images from the deeper and more complex regions of the margin. To overcome these deficiencies, three ships, the Fred Moore from UT, the Oceanus from WHOI and Dawson from BIO were used to form a 13-km synthetic aperture.

Because of equipment availability and ship scheduling, the seismic data acquisition equipment available was far from optimum. The Fred Moore was equipped with source and receiving arrays, while the Dawson had only a source array, and the Oceanus was equipped with only a receiving array (Table I).

Using the equipment available, the ships were positioned with the Dawson in the lead, 6 km in front of the Fred Moore, while Oceanus followed the tail buoy of the Moore

TABLE I

LASE ACQUISITION EQUIPMENT

DAWSON

1	Bolt 800 Airgun	2,000 in^3		
1	Bolt 1500 Airgun	1,000 in^3		
	Total	3,000 in^3	@	2000 PSI

MOORE

1	Bolt 800 Airgun	2,000 in^3		
1	Bolt 1500 Airgun	1,000 in^3		
	Total	3,000 in^3	@	2000 PSI

LRS
48 group streamer
70 m group spacing
30 m active / 40 m dead
3,360 m total active length

DFS IV Data Recording System

OCEANUS

SIE
24 group streamer
100 m group spacing
50 m active / 50 m dead
2,400 m total active length

WHOI Instantaneous Floating Point Data Recording System

array (Figure 2a). Seismic sources were fired alternately by the Dawson (on the minute) and Moore (on the half-minute). Both the Moore and Oceanus received and recorded seismic data for all the shots.

When Moore fired, it would acquire conventional CDP data in the offset range of 0 to 3.6 km and Oceanus would acquire data with source-receiver offsets of 3.6 to 6.0 km. When Dawson fired, Moore would record data for the source-receiver offsets of 6.0 to 9.6 km and Oceanus for the 10.0 to 13.0 km range. For safety, Oceanus remained slightly behind the Moore tailbuoy. This precaution and the space occupied by the ships themselves resulted in a minor loss of offset coverage.

The offset coverage of each array varied along the track as each ship moved slowly with respect to the others. The distance between the ships at every shot was determined using Mini Ranger. Two other ranging systems, Del Norte and Raydist failed, due to space limitations on proper antenna placement. The master Mini Ranger unit was aboard the Dawson with slave units on Moore and Oceanus. Consequently, there is no direct range measurement for Moore to Oceanus. This data had to be interpolated from the Dawson to Moore and Dawson to Oceanus range data.

Shot times were determined using identical National Bureau of Standards Geostationary Operational Environmental Satellite clock receivers (True Time) and back-up Systron Donner oscillators. Identical Loran-C units were also aboard all ships and used to steer the desired course. All timing, range and navigation information were logged on separate digital data logging systems for future use.

Initially it was planned to deploy a 4,000 cu.in. source array composed of a 2,000 cu.in., a 1,000 cu.in. and 2-466 cu.in. Bolt airguns. However, because of towing difficulties only the 2,000 cu.in. and 1,000 cu.in. airguns were deployed. Throughout the CDP profiling both source ships used this two-gun source array (see Table I).

After overcoming initial difficulties in keeping the ships on track and at the proper distances with respect to one another, we were able to acquire four large aperture dip lines and two strike lines for a total of about 900 line km. LASE Line 6, which we report on here was shot directly over USGS Line 25 (Figure 1) extending from just offshore Atlantic City to the base of the continental rise. This line received the highest acquisition and processing priority.

2. Expanding Spread Profiles

An expanding spread profile is a Common Mid-Point reflection/refraction survey with source-receiver offsets up to 100 or more kilometers. In this mode of acquisition the shooting and receiving ships steam away from (or towards) a common mid-point on a fixed pre-determined course (Figure 2b). The shooting ship fires and relays the shot instant to the recording ship via radio. Seismic data is recorded aboard the receiving ship using a multi-channel array and distance is measured using Raydist, Mini Ranger, or Loran-C (for a detailed description see Stoffa and Buhl, 1979). In addition to the LASE CDP lines, 9 Expanding Spread Profiles were successfully acquired along Line 6 (Figure 1).

Two expanding spread profiles were acquired at each of four geographic locations. One profile was acquired using the LASE airgun source array (enhanced by adding two 466 in^3 airguns), and the other using 25-kg explosive charges, timed to go off at or near the sea floor. The ESPs were paired for several reasons. While the explosive sources were intended to, and did, produce deeply penetrating arrivals, the airguns could be fired more frequently. Also, with airgun ESPs the closest offsets obtained were much smaller, producing greater resolution in the reflection data from the sedimentary column. In addition, these data sets enable a direct comparison of ESP results with both types of sources,

providing an important baseline in the planning of future ESP work in areas where no explosive permits can be obtained.

For the explosive profiles, the shooting ship, Dawson, fired 25 kg explosive charges at 10 minute intervals. These were recorded by the receiving ship, Moore, using a digitization interval of 4 ms, and a 48-channel array with 70 m group spacing. The lines were run at a combined ship speed of 18 km/hr and resulted in contiguous offset coverage for each shot, providing essentially 100% coverage at the 70 m group spacing. The explosive ESP lines ranged from 70 to 110 km in length and were designed to provide structural control over the entire crustal thickness, complementing the deep CDP reflection profiles.

The airgun profiles were acquired using a one-minute shooting schedule. During this time, the ships separated only 300 m, resulting in a considerable overlap in offset coverage. In addition to providing improved resolution of the shallow structure, the profiles provided useful large offset refraction data for comparison with the explosive profiles. By combining the closely spaced shots into 50 m source-receiver offset 'bins' during processing, the signal to noise level improved significantly and first arrivals were observed for offsets up to 70 km.

The ESP profiles were located to sample the continental margin at key locations: ESPs 1A ("A" for airgun), 2 and 2A were the most landward, located on what was thought to be continental crust; ESPs 3 and 3A were located at the East Coast magnetic anomaly; ESPS 4 and 4A were at the Outer Carbonate Bank; and, ESPs 5 and 5A were located on oceanic crust.

III. DATA ANALYSIS - CDP DATA

1. Timing and Range

The two LASE recording ships, Moore and Oceanus, recorded the multichannel seismic data digitally on ½-inch, 9-track tape. The Moore recorded 48 channels in SEG-B format, using the L-DGO DFS IV data system. The Oceanus recorded 24 channels in a modified SEGY format. In addition to the actual seismic data tapes, shot and record time, navigation and the distance between ships also were recorded digitally on magnetic tape. These tapes were transcribed into a modified SEGY format and plots made of the raw timing and distance data. Errors in the data were found by inspection and corrected.

Typical of the errors detected were jumps in the satellite-derived time when the satellite receiver switched (inexplicably) from the East to the West satellite. These errors were easily detected. Incorrect range measurements were also intermittently logged. These appeared as spikes in a distance versus time of day plot and were corrected by linearly interpolating a value from adjacent good measurements.

Figure 3 shows plots of the minimum and maximum offset range for all of Line 6 for Moore to Oceanus (4-6.8 km), Dawson to Moore (6.8 to 10 km), and Dawson to Oceanus (10 to 13.4 km), for both the Mini Ranger data and ranges derived from Loran-C time delays. The ranges derived from Loran-C are in good agreement with the Mini Ranger ranges near shore, but they diverge as the line moves further offshore. The scatter in the Loran-derived ranges is about 50 m, which is reasonable since the resolution of the Loran receiver used was .1 μsec or $\sim$30 m.

2. CDP Gather

Because of the unusual profiling configuration (shown in Figure 2a); i.e., two shooting ships and two recording ships, the data were considered to result from four separate sub-profiles. These were: 1) Moore shooting, Moore recording; 2) Moore shooting, Oceanus recording; 3) Dawson shooting, Moore recording, and 4) Dawson shooting, Oceanus recording. Each of these sub-profiles was separately CDP-gathered with its own CDP numbering scheme. This was done using the edited master data-logger tape. Ranges from the shooting to recording ships and shot minus record time static shifts were read from the data-logger tape and input to the gathering program for each shot.

To account for the different active group spacings of the two recording arrays, Table II, the CDP spacing was arbitrarily chosen beforehand to be 50 m for each of the four gathering operations. The four sub-profiles, summarized in Table III, were merged by combining the individual gathers at common geographic coordinates into "super" CDP-gathers. During this operation, the final CDP numbering system was adopted which placed LASE Line 6 CDP 1 at 39°18' north latitude, 74°00' west longitude. Each CDP is centered at a distance of 50(CDP-1) m along a line running 126° from CDP 1. The data traces within each super gather were sorted into increasing offset order to facilitate plotting the gathers on a true offset scale. At the conclusion of the gather-merge operation, LASE Line 6 consisted of 6000 CDP gathers, each one of which was approximately 48 fold.

TABLE II

LASE ACQUISITION PARAMETERS

MOORE	OCEANUS
48 trace	24 trace
70 m groups (30 m / 40 m)	100 m groups (50 m / 50 m)
20 sec data length	20 sec data length
4 msec sampling	4 msec sampling

TABLE III

LASE CDP SORT SUMMARY

MOORE-MOORE CDP SORT	MOORE-OCEANUS CDP SORT
146 m shot spacing	146 m shot spacing
258 m offset to near group (constant)	varying offset to near group
∿0-3.5 km offsets	∿4-6.5 km offsets
50 m depth point spacing	50 m depth point spacing
∿16 fold	∿7 fold

DAWSON-MOORE CDP SORT	DAWSON-OCEANUS CDP SORT
varying shot spacing	varying shot spacing
varying offset to near group	varying offset to near group
∿6.5-10 km offsets	∿10.5-13 km offsets
50 m depth point spacing	50 m depth point spacing
∿16 fold	∿7 fold

3. CDP Stacks

Before the merged LASE gathers were subjected to any additional processing, variable area displays were made of the data as a function of source-receiver offset (Figure 4). Usually, three CDPs were plotted for each time-distance origin, representing the maximum data fold and a 150 m CDP bin spacing.

Figure 4 shows CDP gathers from two areas of interest. On the left are data near the East Coast magnetic anomaly, while on the right are data from the Outer Carbonate Bank area. Visually, the seismic arrivals appear remarkably continuous from one ship's array to the other. On the shelf, wide angle reflections and refractions are observed, as are deep reflections at about 6 to 9 seconds of two-way normal time.

All the data were displayed in a similar fashion and visually inspected for timing and range errors. Several incorrectly timed shot points were included in the gathers and appeared as data with a static time shift. Also, it was discovered that the Dawson to Oceanus range data were incorrectly used during the initial CDP merge. (In all subsequent displays and processing steps described here these data were excluded, since to recover the correct offsets, the data has to be re-gathered.)

After editing, standard hyperbolic X-T semblance velocity scans were made to define the stacking velocities. Semblance was computed for the offset ranges 0-4 km and 0-10 km. Three CDPs were used in each velocity scan and the calculation was done every 20 CDPs. Velocities of 1400 to 6000 m/sec were computed at an interval of 50 m/sec (Figure 5).

Both the 0-4 km and 0-10 km hyperbolic velocity scans were used to define stacking velocities. The 0-10 km scans were unusable for the shallow part of the section (less than four seconds of two-way normal time) because of the failure of the hyperbolic traveltime assumption and the presence of refractions. Consequently, the 0-4 km scans were used for the shallow part of the section and the 0-10 km scans were used for the deeper part. In all cases, Grow's (USGS unpublished) velocities for USGS Line 25 were used as a guide in the interpretation.

After stacking velocities were defined, the CDP gathers were corrected for normal moveout and displayed. This was done approximately every 100 CDPs for quality control and to define post normal moveout mutes (Figure 6). The mutes were defined in table form and were spatially interpolated between analysis points along the line when the data were stacked. In most cases, below about 4.5 seconds of two-way normal time, offsets greater than 4 m were included in the CDP stack.

Before stack, gain proportional to arrival time ($T^{1.5}$) and trace equalization (based on the mean absolute value) were applied to the data. In order to collapse the source waveform, prediction deconvolution was done using a 200 msec filter with a 30 msec prediction distance and 1% white noise. A design gate of 5500 msecs, beginning at 2500 msecs traveltime and varying linearly with offset, was used to avoid water-borne energy.

The CDP data for source-receiving offsets of 0-10 km were stacked individually with the stacking velocities spatially interpolated between the analysis points. After stack, many post-processing sequences were tried. The sequence used in Figure 7 included a zero phase time varying band pass filter whose cut-off frequencies were:

12	and	50	Hz	at	0	msecs
10	and	40	Hz	at	3000	msecs
6	and	25	Hz	at	5000	msecs
4	and	15	Hz	at	9000	msecs
4	and	10	Hz	at	14000	msecs

In this display, which has the velocity functions derived from the ESPs superimposed, a running mix of nine traces was used to improve the definition of the deep structure, followed by spatial decimation by a factor of 3. Thus, a CDP spacing of 150 m was used for display but each CDP is now

averaged over 450 m. Post-stack predictive deconvolution was also applied to reduce both source- and water-column reverberation. Automatic gain control, using a response time of 750 msec was used for display and the geometric distortion caused by variations in water depth was removed through knowledge of the seafloor two-way traveltime and assuming a propagation velocity of 1.5 km/sec.

In Figure 7, it is possible to trace the top of the deep 7.2 km/sec layer from ESP 1, where it is found to lie at a two-way normal time of about 7.6 seconds to ESPs 2 and 3 where it is present at times greater than about 8.0 seconds (see Part II for a detailed interpretation). On the right part of the section, oceanic basement can be visually traced landward to about CDP 3300 and by correlation with ESP 5 it can be followed to the area just seaward of the Outer Carbonate Bank Complex. Figure 8 is a schematic interpretation of this section showing the major geologic horizons observed in the record section.

The identical processing sequence (pre and post stack) and display was used for the conventional CDP data acquired by the Moore for the offsets of 0-3.5 km. Figure 9 is a detailed comparison of the two record sections from the outer carbonate bank area. In this figure the additional signal to noise improvement provided by using the larger offset data (lower panel), is evident in at least two ways. First, the

residual multiple energy has been reduced to the extent that part of the prograding carbonate sequence can be traced from CDP 2100 to 2450 at two-way times of 4.0 to 4.5 seconds. An even shallower reflection at 3.8 seconds of traveltime under the reef complex can now be traced landward through the multiple to CDP 2100. It is also clear that the top of the prograding carbonate sequence is better delineated in the 0-10 km stacked section. Because of the post-normal movement mutes applied, the full 10 km aperture is not being used at these two-way times, but sufficient additional primary reflection energy is being included in the stack to give significantly better multiple attenuation and signal to random noise improvement.

The LASE Line 6 data were migrated (after stack) using the phase-shift method (Gazdag, 1978; Dubrulle and Gazdag, 1979). The phase shift method is a modification of the more common f-k migration (Stolt, 1978) which eliminates the extreme stretch necessary to put the data into a constant velocity versus depth form.

We migrated LASE Line 6 from CDP 1000 to CDP 3000, a traverse of 100 km, using data from 0 to 16 sec. The velocity structure was a combination of converted stacking velocities in the upper part of the section tied to refraction data from the expanding spread profiles for the deeper layers. Figure 10 is a comparison of the migrated and

unmigrated data from the basement fault area. In the migrated record section (right), the long diffraction events present in the stacked section (left) have been substantially reduced. It is now quite clear that at 6.5 seconds of two-way time, CDP 1250 marks the edge of a major basement normal fault. Shallower faulting at 5.8 seconds of two-way time is also well defined in the migrated section. On the lower right of both sections the downward thrown block is clearly observed.

The stacked, migrated data were also converted from two-way normal time to depth. The interval velocity functions used for depth conversion were those which modeling showed to correspond most closely to stacking velocities picked from the 0-4 km data semblance scans. These velocity functions were also constrained by analysis of the ESP results, where applicable. Figure 11 is a detailed display from the outer carbonate bank area with interval velocities annotated on the record section.

Figure 11 shows that in the region of the upper Jurassic carbonate bank at CDP 2400 there is an abrupt increase in compressional velocity across the Upper Jurassic horizon (the top of the carbonate bank) at 3.7 km depth, separating layers having velocities of 3.7 and 5.3 km/sec, respectively.

A general observation regarding the interval velocity distribution within each seismic unit above the Jurassic carbonate bank is the steady decrease in velocity array from the shelf edge. The most obvious, dominant effect is probably the decrease in the thickness of the overburden and, perhaps also the increasing predominance of finer grained terrigenous sediments.

The velocity data also confirm the presence of the Turonian-Cenomanian unconformity. In the COST B-3 sonic log there is an abrupt increase in interval velocity (about 700 m/sec) at about 2.5 km depth. In Figure 11, COST B-3's location would project to CDP 2170, where the derived interval velocity increases from 2862 to 3645 m/sec at approximately 2.6 km depth, in good agreement with the well results.

IV. ESP DATA

1. Basic Processing

For all nine ESPs, time and source-receiver offsets were displayed and corrected. For the airgun profiles little or no timing corrections were necessary. For the explosive profiles significant shot instant time corrections had to be made. Because of the failure of Raydist, source-receiver offsets for the near offset ranges (0-40 km) were determined using Mini Ranger. As the offset increased, latitude and longitude measurements from Loran-C were incorporated into the distance determination (Loran time delays and Mini Ranger were calibrated for the near offsets, and then Loran used after the Mini Ranger's range was exceeded).

The separation rate of the ships during the airgun ESPs was about 18 km/hr or 300 m/minute. Firing on a one-minute schedule and using a 3.36 km array generated about 90% data overlap in the source-receiver offsets sampled. Rather than maintain the original data fold, the data traces were summed into 50 m offset bins and scaled by the number of traces in each bin. Instead of a simple mix, each data trace was linearly "moved out" with a reducing velocity of 8 km/sec before summing to correct for the difference in distance between the nearest 50-m bin mid-point and the data traces'

true offset. This procedure reduced the volume of data and increased the signal to random noise level by a factor of 3.

Several displays of the ESP data were made. For the explosive expanding spread profiles, which extend to 100 km, both normal and reduced (5.5 km/sec) traveltime plots were generated, while the airgun ESPs could be displayed more readily at one time-scale. In all cases pre-display processing included band-pass filtering and automatic gain-control.

2. Derivation of Velocities

Interval velocities were derived from the LASE ESP data by analyzing seismic travel time trajectories in both the X-T and tau-p domain. Both near-vertical incidence reflections (for the airgun profiles) and wide angle reflections and refractions were used. The airgun profiles were initially analysed in the tau-p domain and the velocity structure was refined by raytracing and comparison with the observed T(x) data. Using the airgun results for the shallower part of the section, the explosive ESPs were then fitted by an iterative process of comparison with ray-traced arrivals in order to obtain interval velocities for the deep post-stack section. The seismogram density afforded by the multichannel array allowed the use of many phases in addition to the usual first arrivals.

a. Airgun Expanding Spread Profiles

We describe in detail the analysis of ESP 3A (Figure 12a) to illustrate the method of analysis for the airgun Expanding Spread Profiles. This profile was transformed to the tau-p domain using data with source-receiver offsets of 0-20 km and a ray parameter sampling interval of 2 msec/km. The locations of critically refracted and postcritically reflected arrivals were digitized and inverted to obtain V(Z) by the slope-intercept or "Tau-Sum" recursion method (Diebold & Stoffa, 1981). By picking closely spaced tau-p points, an accurate representation of velocities and gradients in the upper seven kilometers of the section was obtained. The tau-p interval velocity model we derived was smoothed and then verified by comparing the ray traced T(X) arrival times with the original data.

Next, T^2-X^2 solutions were calculated for reflections with two-way normal times of 2 to 6 seconds. The very wide angles of reflection that were available precluded the effective use of Dix's approximation for velocity determinations. The "straight line" assumed in Dix's approximation to T^2-X^2 data is actually a curve with gentle negative curvature, becoming more curved as the velocity contrast increases. If straight lines are fitted at near-vertical incidence, most of the data are unused, resulting in

a loss of velocity resolution at depth. The curvature in the T^2-X^2 data can be eliminated if each layer is isolated and treated as a single constant-velocity layer. This is accomplished by solving each layer step-wise from the top down and using the solutions from the overlying layers to "strip" off all the time to a given reflector that is not in the immediately superjacent layer, as described by Le Pichon et al. (1968).

Before the T^2-X^2 analysis of ESP 3A was performed, the data were phase velocity filtered to minimize the interference of the seafloor reflection and multiples. After phase velocity filtering, the data were deconvolved and displayed (Figure 12b). Compared to the original data, the wide angle reflections are readily observed and it is these events which were used in the T^2-X^2 velocity analysis.

Finally, the derived velocity functions were reconciled and rechecked by raytracing and comparison with the original airgun and explosive ESP data. As shown in the composite velocity profile (Figure 13), the tau-p results from 0-4 seconds show more resolution in velocity than the T^2-X^2 solution, though the two results match well overall. The tau-p solution, however, produced no information as deep as the low velocity zone between 5 and 6.5 seconds. In this region, the T^2-X^2 and explosive T(X) results match quite well. Below 6.5 seconds, all the information comes from the explosive ESP results described below.

One interesting feature is the occurrence of the low velocity zone between 5 and 6.5 seconds of two-way normal time. This zone is obtained from the T^2-X^2 reflection data and does not violate the results obtained from the explosive ESP refraction data. To help establish the validity of this result, the final interval velocity-depth function was converted to stacking velocities and two-way normal times. This conversion was accomplished by raytracing the velocity model (Figure 13), and finding the best-fitting hyperbolae over the area of interest by least squares. In this case, 20 km were used in the least squares fit. The ESP 3A data were then corrected for normal moveout and displayed (Figure 14a). The NMO corrected reflection data now appear on nearly horizontal X-T_o trajectories indicating that the stacking velocities are correct.

To test the sensitivity to the low interval velocity zone, the stacking velocities were re-computed using, instead of the low velocity, an interval velocity of 6 km/sec, which is equivalent to that just above the low velocity zone. The data were again corrected for normal moveout and compared. Figure 14b is a detailed comparison of the moved out data for the reflection at 6.5 seconds. The data on the left (low velocity zone) follow a nearly horizontal trajectory while the data on the right (continued high velocity) are clearly undercorrected. This is exactly the error that we would

expect from using the higher stacking velocity associated with the incorrect high interval velocity for this zone.

It is apparent in Figure 14b that the stacking velocity obtained for the low velocity zone is still a bit too high. The reason for this is seen in Figure 13, where the T^2-X^2 and explosive ESP derived velocity functions are superimposed. The T^2-X^2 inversion, obtained from the reflector itself, and thus confined to offsets from 0-20 km yields a velocity function which is lower, on the average, than that produced by the explosive ESP inversion where the derived velocity function is controlled by refractions seen from offsets of 50-90 km. The resulting difference in the raytraced derived stacking velocities (4525 m/sec vs. 4610 m/sec) causes the residual NMO in Figure 14b (left). The implication of this is that the velocity structure within the low velocity zone is more stratified in velocity than the simple functions shown in Figure 13, and that the velocity differences are thus angle- and, therefore, offset-dependent.

Airgun ESP 4A (Figure 15a) was analyzed in a similar way. First, the data were was transformed to the tau-p domain, using offsets of 0 to 20 km. The data were deconvolved in tau-p, displayed (Figure 15b), and inverted using the Tau-Sum method. For this profile the velocity depth structure was refined by moving out the tau-p data (Figure 15c), until the event trajectories became horizontal

(Stoffa et al., 1981). X(T) raytracing was also performed and the event times reconciled with the data for both the airgun and explosive profiles.

ESPs 1A, 2A and 5A were analyzed in a similar fashion. The derived velocity-depth functions, after being combined with the explosive profile results, are summarized in Figure 16.

b. Explosive Expanding Spread Profiles

ESP 2 was acquired closest to the coastline. Locating its position on the reflection profile (Figure 7) confirms the presence of continental basement beneath the sequence of shelf sediments. We observe a steep initial velocity gradient with a refraction velocity of 4.5 km/sec reached by 2.5 km depth (Figure 16). Beyond 35 km distance (Figure 17a), a first arrival of velocity 6.4 km/sec is present which begins to weaken beyond approximately 50 km, indicating a low velocity zone below this refractor.

Between 60 and 70 km we see two sets of faster arrivals: 7.2 km/sec at a reduced time of around 4 seconds and 8.0 km/sec approximately half a second later, though the latter velocity is not well constrained. These are presumed to be at or near the critical distances and the arrivals with

similar apparent velocities observable at closer ranges, particularly around 40 km, are probably precritical reflections. This interpretation is consistent with a weak low velocity zone below the previous refractor. We note that the presence of the 8.0 km/sec event behind the 7.2 km/sec arrivals indicates that the latter is a true refraction, not a reflection branch between the 6.4 km/sec and the 8.0 km/sec refractions.

The principal features of the structure, as shown in the model (Figure 16), are fairly well defined. There is a sequence of high-velocity sedimentary layers culminating in the refractor of 6.4 km/sec at approximately 11 km depth. This is a thin layer beneath which there is a slight decrease in velocity. The model used here has a 6.2 km/sec velocity increasing to 6.6 km/sec over 9.5 km of depth, which are values appropriate for continental basement. Below this is a lower crustal layer approximately 6 km thick with velocity probably greater than 7 km/sec underlain by mantle. It should be emphasized that the use of uniform velocity gradients and of discontinuities in the model is for computational and modeling convenience; the refraction data place little constraint on the sharpness of boundaries. The observation of precritical reflections, however, particularly from the top of the lower crustal layer and, to a lesser extent, from the mantle, suggest that these boundaries are in fact quite sharp.

ESP 3 is still on the continental shelf, but the seismic reflection profile (Figure 7) shows that the continental basement has disappeared. There are some significant differences between this profile (Figure 17b) and the corresponding model (Figure 16) compared to ESP 2.

First, the arrival with velocity 6.4 km/sec is no longer present and the fastest sedimentary refractor is approximately 5.7 km/sec. Again, this refractor fades indicating the absence of a significant velocity gradient. The refraction traveltimes do not require a low velocity zone but analysis of the reflection data for ESP 3A does. Consequently, we have included the low velocity zone in our final model and the predicted traveltimes superimposed on the record section of Figure 17b agree with the observed arrivals. Subsequent velocities are masked or out of range and the next clear arrivals appear to be on a strong reflected branch from a 7+ km/sec refractor corresponding to the lower crustal layer seen in ESP 2. These arrivals dominate the section beyond approximately 40 km, indicating that this layer has thickened. In fact, a P_n arrival of velocity near 8 km/sec cannot be positively identified so the depth to mantle shown in Figure 16 is speculative. It is based on the high amplitudes seen at approximately 80 km range and the absence of any observed P_n first arrivals.

ESP 4 was shot along the continental slope (Figure 7). We see from the record section (Figure 17c) and model (Figure 16) that the velocity increase with depth is much greater than that on the shelf. The most striking feature is a high velocity (5.6-5.7 km/sec) refractor only 3 km beneath the sea floor with a very marked low velocity zone immediately below. The position of the offset arrivals suggests a mean velocity within the low velocity zone not much greater than 5 km/sec over a thickness of approximately 6 km.

Again, there is a strong refraction at a velocity of 7.2 km/sec. The critical distance, which appears to be about 50 km, suggests a substantial velocity gradient below the low velocity zone which is consistent with the concentration of energy between 50 and 70 km. A P_n first arrival is not seen. A later arrival, tentatively identified as P_n, is observed at approximately 60 km range at the time and critical distance corresponding to a thickness of 7 km for the lower crustal layer.

ESP 5 was acquired along the continental rise over crust which is definitely oceanic but probably greatly influenced by the nearby margin. The structure appears to be characterized by continuous velocity increase without strong discontinuities; in particular, there is no obvious transition from the sedimentary column to basement. There

is, however, a clear break and triplication at 30 to 45 km with velocity increasing rapidly to, again, approximately 7.2 km/sec (Figure 16). A weak P_n first arrival is present between 80 and 100 km giving a thickness of approximately 7 km for the lower crustal layer.

CONCLUSION

The LASE experiment succeeded in proving the feasibility of acquiring large synthetic-aperture CDP data even when the acquisition equipment available is far from optimum. The stacked 0-10 km CDP data shows an improved signal to noise ratio compared to the stacked 0-4 km Moore-to-Moore data over the deep part of the section. This comparison is appropriate since the same source arrays were employed.

Of particular importance is that the 7.2 km/sec layer, determined from the ESP data, can now be detected for the first time in the stacked record section. Although this event is not readily observed on USGS Line 25, it is primarily because of the correlation with the new ESP data that we are confident in our interpretation of this event in the 0-10 km stacked section.

Overall, USGS line 25 exhibits a better signal to noise ratio for most parts of the section. We attribute this primarily to the differences in the source array used. In the USGS line a tuned 2,000 cu.in. source array was used compared to the detuned LASE array of 3,000 cu.in.

The ESP data, both airgun and explosive, have proved invaluable in deriving the geologic interpretation described in Part II of this paper. The airgun profiles, which were

particulary well suited for the shallower part of the section, also proved useful for deriving information about the deep part of the section. The additional signal level provided by the nine-fold combination of traces in these densely shot profiles indicates that even in seismically difficult areas significant penetration is possible using airguns. Employment of a higher energy source array should make this approach viable in areas where explosives would normally be employed.

The LASE explosive ESP profiles provided most of the information for the deep part of the section, particularly the observation of the 7.2 km/sec reflection event. Because of the sparser shot spacing, these profiles poorly resolved the shallow part of the section, but the higher energy source did provide sufficient signal level so that wide angle reflection and refraction events could be observed at source-receiver offsets of up to 100 km.

The combination of the large aperture CDP data, with both the airgun and explosive ESPs, has provided a data set, which for deep crustal studies, is significantly more detailed than previously available. It is this combination which leads to the interpretation outlined in Part II of this paper.

The institutions and principal contributors to the LASE Study Group are:

C. Keen, I. Reid, J. Woodside, B. Nichols
Atlantic Geoscience Centre, Bedford Institute of Oceanography
Dartmouth, Nova Scotia, Canada

J. Ewing, P. Stoffa, D. McCowan, J. Diebold, M. Truchan, T. O'Brien
Center for Marine Crustal Studies, Gulf Research & Development Co.
One Blue Hill Plaza, Pearl River, New York

P. Buhl, J. Mutter, R. Mithal, J. Alsop
Lamont-Doherty Geological Observatory of Columbia University
Palisades, New York

J. D. Phillips, T. Stark
University of Texas, Institute for Geophysics
Austin, Texas

M. Purdy, Hans Shouten
Woods Hole Oceanographic Institution
Woods Hole, Massachusetts

This work was supported by grant from the National Science Foundation, OCE 79-22884, and the industrial participants of the Ocean Margin Drilling Program:

Atlantic Richfield
Cheveron
City Service Co.
Conoco
Exxon
Mobil
Penzoil
Phillips Petroleum
Sunmark
Union Oil

and

Gulf Research & Development Company.

REFERENCES

Buhl, P., J. B. Diebold and P. L. Stoffa, "Array Length Magnification through the Use of Multiple Sources and Receiving Arrays;" Geophysics, Vol. 47, No. 3, March, 1982, pp. 311-315.

Diebold, J. B. and P. L. Stoffa, "The Traveltime Equation, Tau-p Mapping and Inversion of Common Midpoint Data;" Geophysics, Vol. 46, No. 3, 1981, pp. 238-254.

Dubrulle, A. A., and J. Gazdag, Migration by phase shift - An algorithmic description for array processors, Geophysics, v. 44, 1979, 1661-1666.

Gazdag, J., Wave equation migration with the phase shift method, Geophysics, v. 43, 1978, 1342-1351.

Grow, J. A., C. O., Bowin, D. R. Hutchinson, "The gravity field of the U.S. Atlantic continental margin," Tectonophysics, 59, 1979a, pp. 27-52.

Grow, J. A., R. E. Mattick, J. S. Schlee, "Multichannel seismic depth sections and interval velocities over outer continental shelf and upper continental slope between Cape Hatteras and Cape Cod, in Geological and geophysical investigations of continental margins," edited by P. W. W. Dickerson, U. S. Geol. Surv. Circular, 833, 1979b, pp. 117-125.

Klitgord, K. D. and J. C. Behrendt, in "Geological and Geophysical Investigations of Continental Margins," J. S. Wtkins, L. Montadert and P. Dickerson, editors, Amer. Assoc. Petrol. Geol. Memoir, 29, 1979, p. 85.

Le Pichon, X., R. Houtz, and J. Ewing, "Deep-sea sediment velocity determination made while reflection profiling," J. Geophys. Res., 1968, pp. 2597-2614.

Sawyer, D. S., B. A. Swift, J. G. Sclater, and M. N. Toksoz, Geology, 10, 1982, p. 134.

Schlee, J. S., Amer. Assoc. Petrol. Geol. Bull., 65, 1981, p. 26.

Scholle, P. A., (ed.), "Geological Studies on the COST B-2 Well," U. S. Geol. Survey Circular, 750, 1977, 71p.

Scholle, P. A. (ed.), "Geological Studies of the COST No. B-3 Well," U. S. Geol. Survey Circular, 883, 1980, 132p.

Sheridan, R. E., J. A. Grow, J. C. Behrendt, and K. C. Bayer, Tectonophysics, 59, 1979, p. 1.

Steckler, M. S. and A. B. Watts, Subsidence of the Atlantic-type continental margin off New York," Earth Planet, Science Letters, 41, 1978, pp. 1-13.

Stoffa, P. L. and P. Buhl, "Two-Ship Multichannel Seismic Experiments for Deep Crustal Studies: Expanded Spread and Constant Offset Profiles," Journal of Geophysical Research, v. 84, 1979, pp. 7645-7660. L-DGO Contribution No. 2860.

Stoffa, P. L., J. B. Diebold and P. Buhl, "Inversion of Seismic Data in the Tau-p Plane," Geophys. Res,. Ltrs., v. 8, no. 8, 1981, pp. 869-872.

Stolt, R. H., "Migration by Fourier transform," Geophysics, v. 43, 1978, pp. 23-48.

Watts, A. B. and M. S. Steckler, in "Deep Drilling Results in the Atlantic Ocean: Continental Margin and Paleoenvironments," M. Talwani, W. Hay and W. B. F. Ryan, editors, Maurice Ewing Series 3, 1979, Amer. Geophys. Union, Washington, DC, p. 218.

Figure 1 Track chart - showing the location of LASE Line 6 and the nine expanding spread profiles. The shaded area defines the location of the East Coast Magnetic Anomaly.

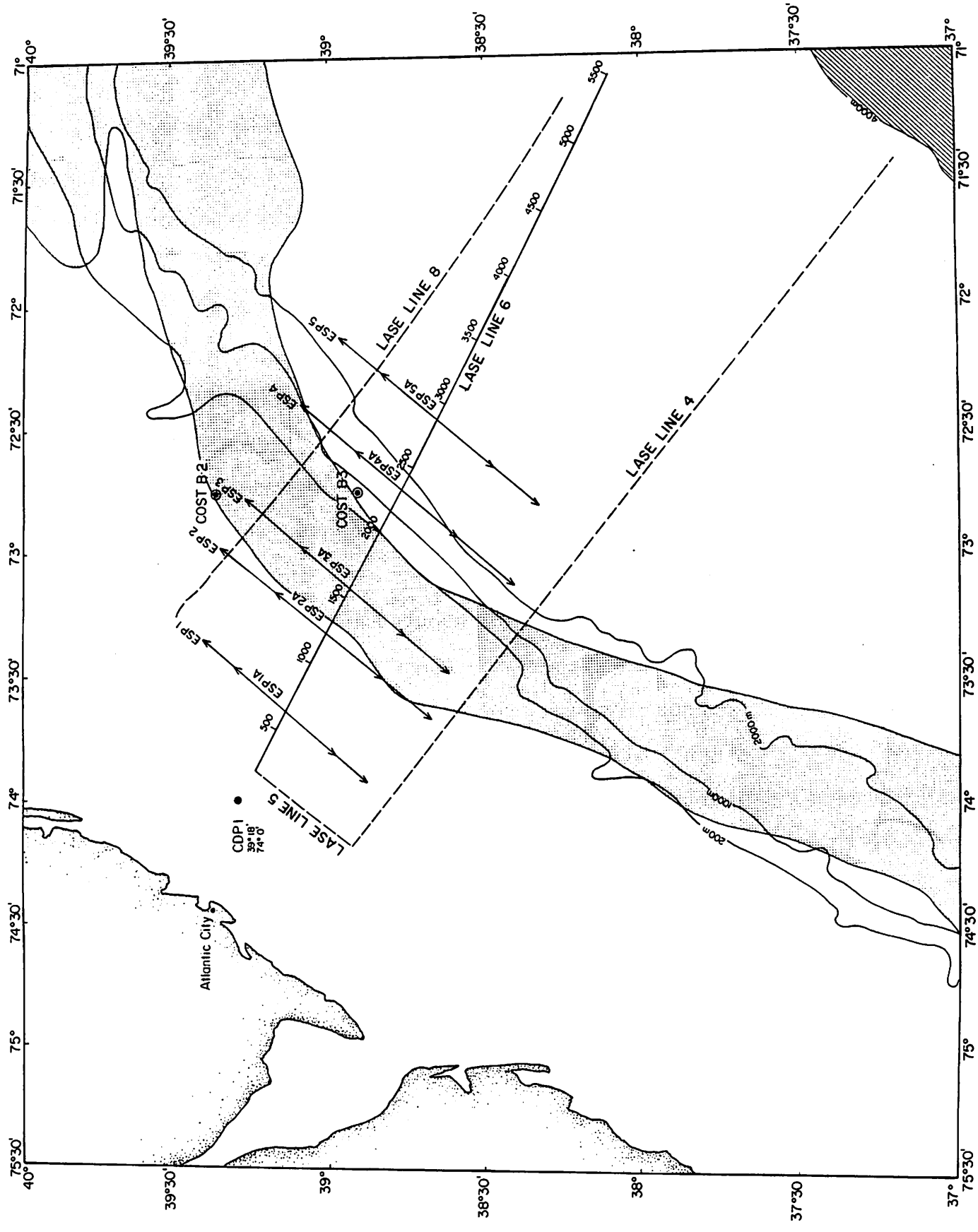
LASE LINE 8
LASE LINE 6
LASE LINE 4
LASE LINE 5
ESP 5
ESP 5A
ESP 4
ESP 4A
ESP 3
ESP 3A
ESP 2
ESP 2A
ESP 1
ESP 1A
COST B2
COST B3
CDP 1
39°18'
74°0'
Atlantic City
200m
1000m
2000m
4000m
500
1000
1500
2000
3000
3500
4000
4500
5000
5500
71°
71°30'
72°
72°30'
73°
73°30'
74°
74°30'
75°
75°30'
40°
39°30'
39°
38°30'
38°
37°30'
37°

FIGURE 1

Figure 2a Schematic diagram of the LASE large aperture CDP profiling plan. The lead-ship Dawson was approximately 6.5 km ahead of Fred Moore and Oceanus followed the tailbuoy of the Moore. Range between the ships was determined using Mini-Ranger. When the Fred Moore would fire its airguns, the Moore and Oceanus would record seismic data. Moore would acquire a conventional reflection record section with offsets of 0 to 3.5 km. At the same time Oceanus would record data with offsets of about 3.6 to 6.0 km. Thirty seconds after the shot from Moore, Dawson would fire its airguns. Then the Fred Moore would record data with offsets from 6 to 9.6 km and the Oceanus would record offsets from 10 to 13.0 km. After initial logistical problems the ships were able to maintain the desired separation and steamed the same line using identical Loran-C receivers for navigation.

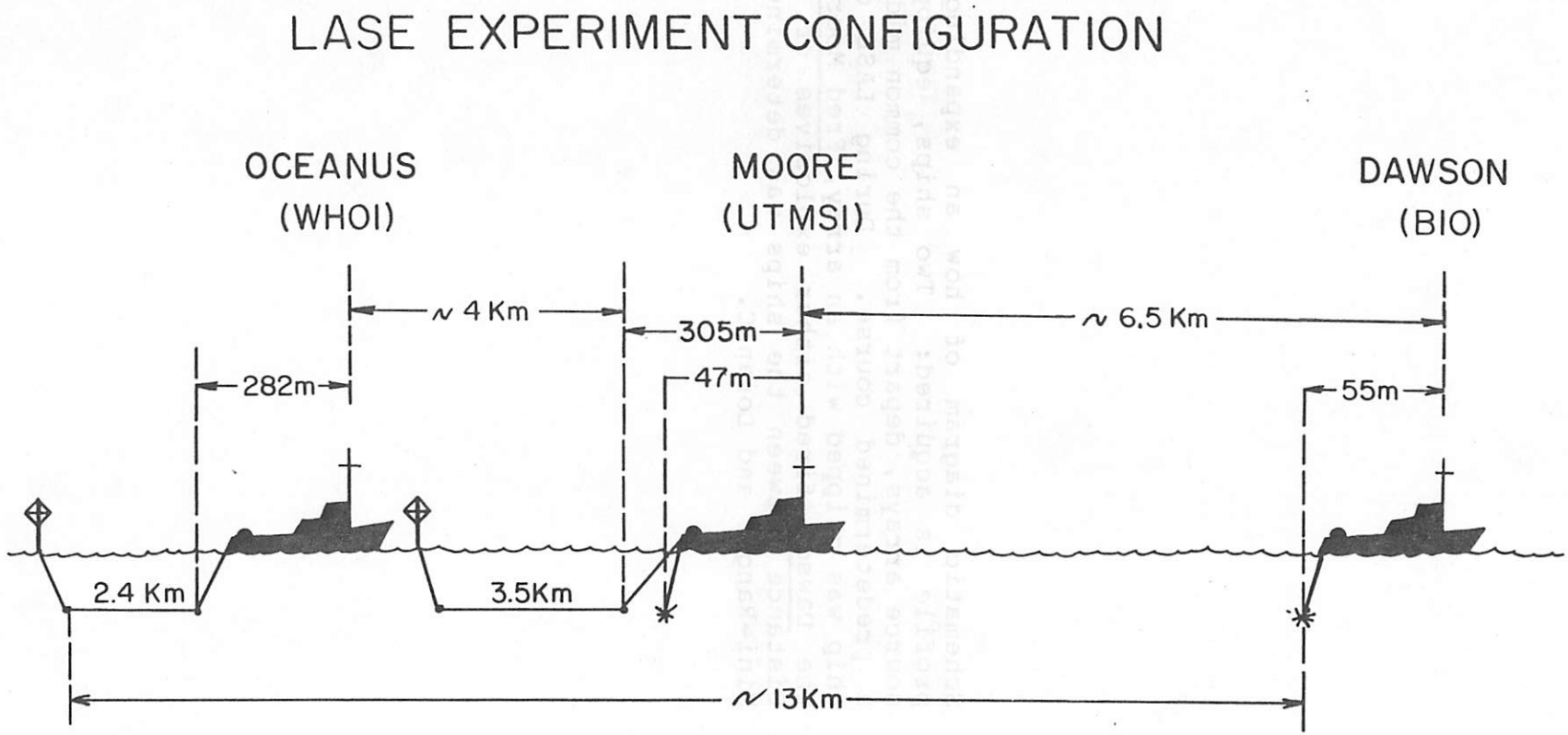
LASE EXPERIMENT CONFIGURATION
OCEANUS
(WHOI)
MOORE
(UTMSI)
DAWSON
(BIO)
~ 4 Km
305m
~ 6.5 Km
282m
47m
55m
2.4 Km
3.5Km
~13Km

FIGURE 2a

Figure 2b Schematic diagram of how an expanding spread profile is acquired: Two ships, equipped with source arrays, depart from the common midpoint on a predetermined course. During LASE only one ship was quipped with an array, Fred Moore, while the Dawson fired either explosives or airguns. Distance between the ships was determined using Mini-Ranger and Loran-C.

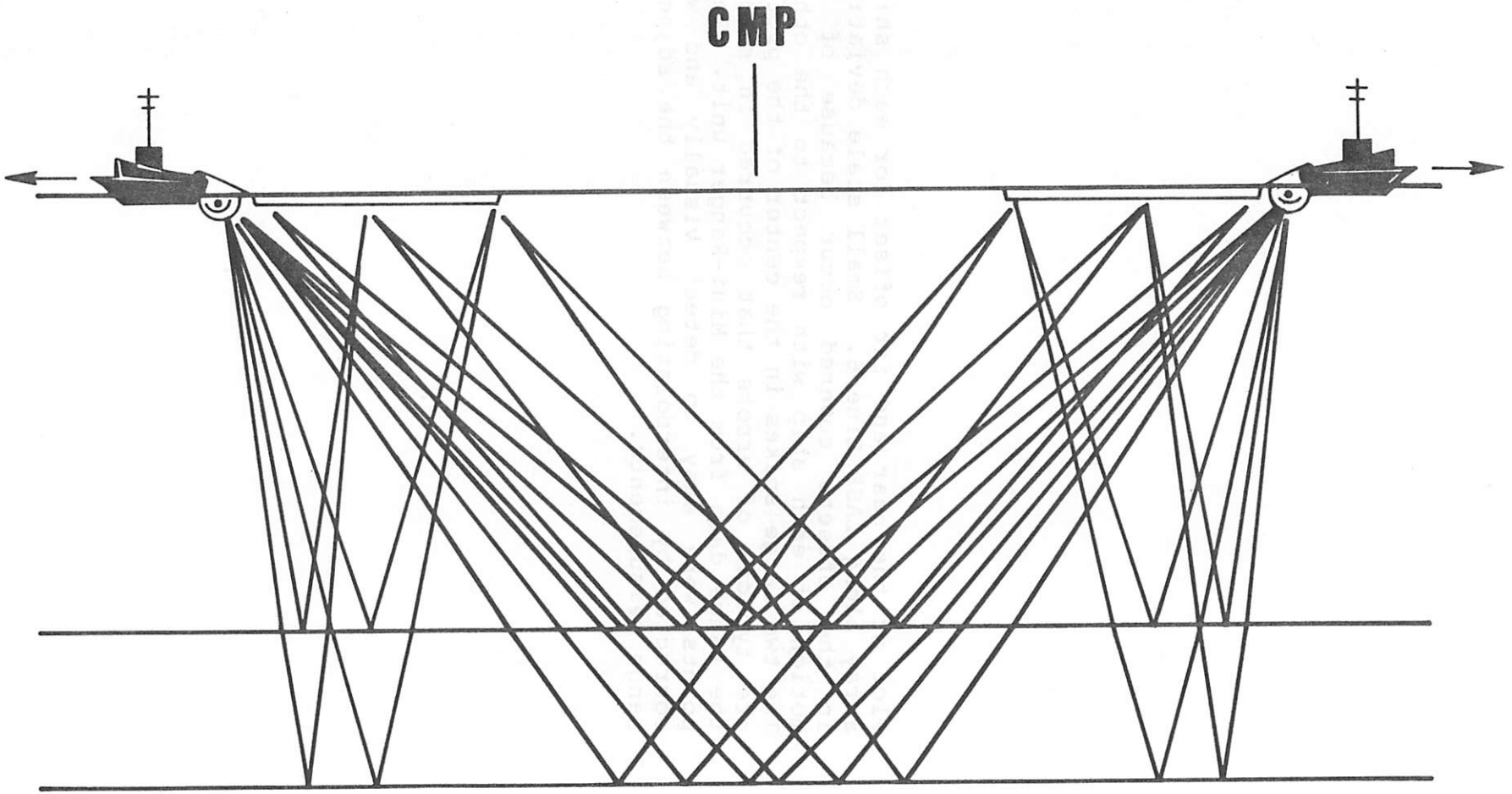

FIGURE 2b

Figure 3 Plot of the near and far offset for each ship's array along LASE Line 6. Small scale deviations in the offsets covered occur because of the motion of each ship with respect to the other. The two large spikes in the center of the profile are typical of errors that occurred in reading the range data from the Mini-Ranger unit. These points were easy to detect visually and were corrected by interpolating between the adjacent range measurements.

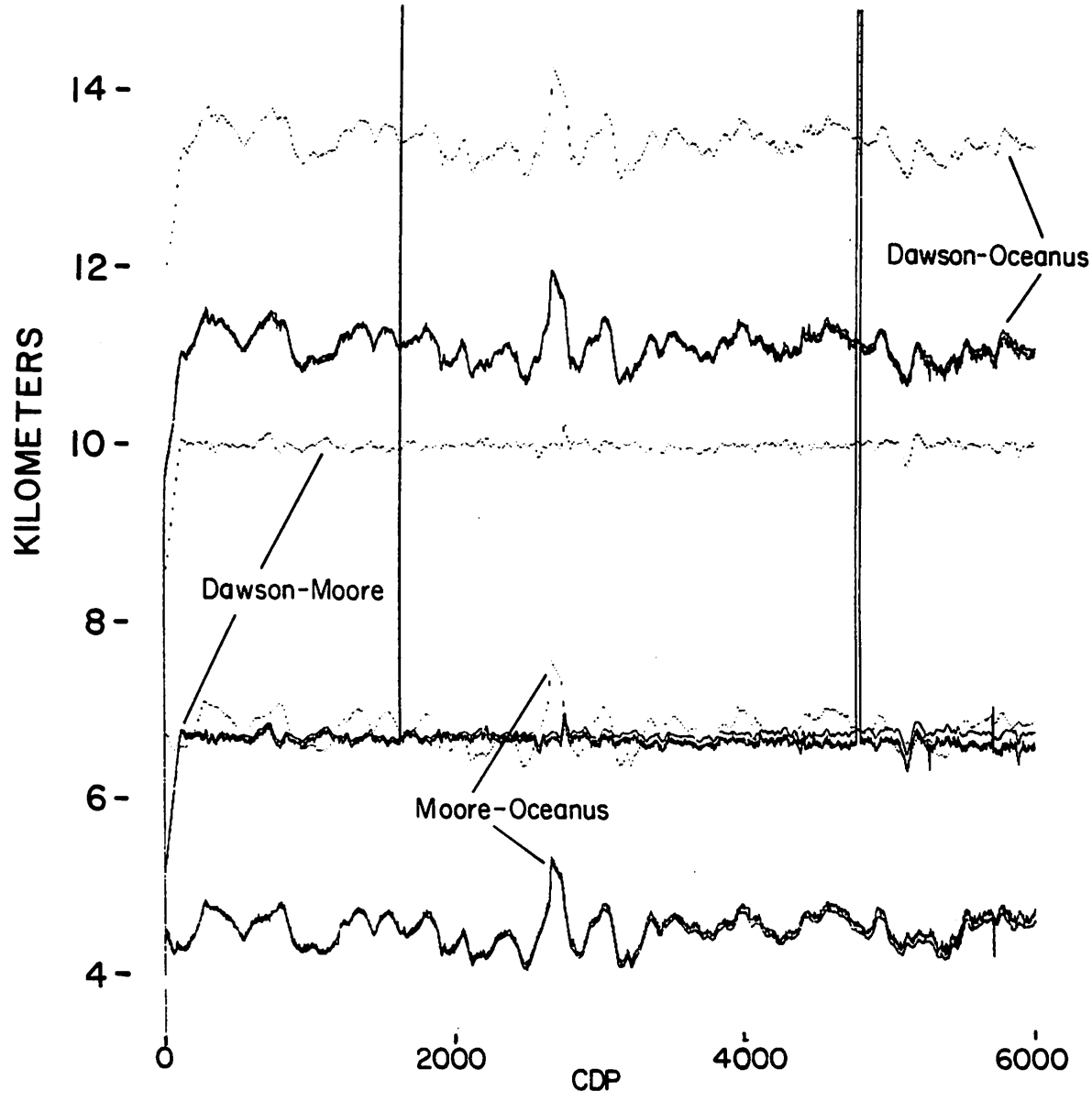
14-
12-
10-
8-
6-
4-
KILOMETERS
Dawson-Oceanus
Dawson-Moore
Moore-Oceanus
0
2000
4000
6000
CDP

FIGURE 3

Figure 4 LASE 0-10 km CDP gathers plotted at their true source-receiver offset from the area of the East Coast Magnetic Anomaly (left) and carbonate bank area (right). Three CDPs are displayed on each panel corresponding to a CDP ground spacing of 150 m.

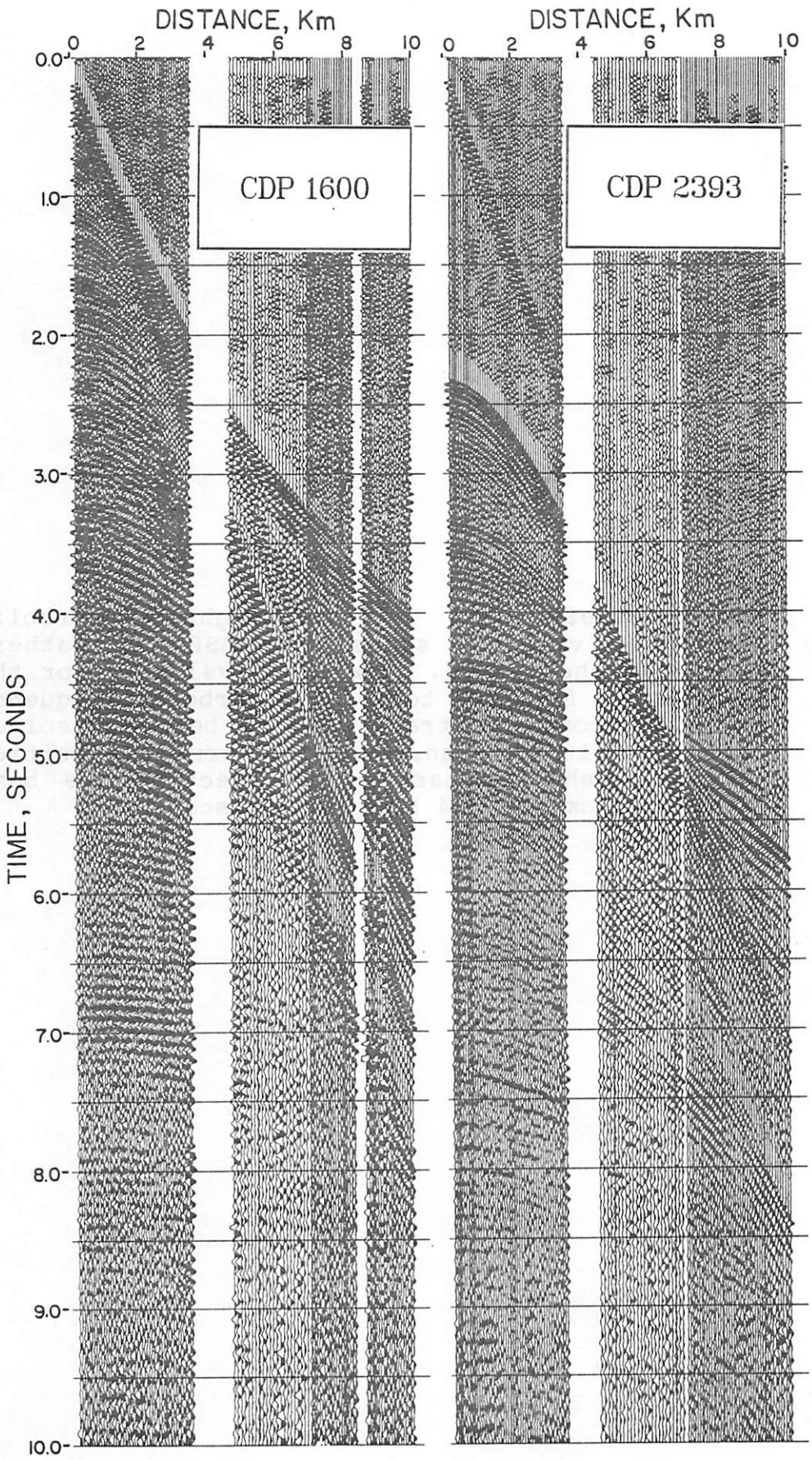
DISTANCE, Km
0
2
4
6
8
10
CDP 1600
DISTANCE, Km
0
2
4
6
8
10
CDP 2393
TIME, SECONDS
0.0
1.0
2.0
3.0
4.0
5.0
6.0
7.0
8.0
9.0
10.0

FIGURE 4

Figure 5 · 0-4 km (left) and 0-10 km (right) hyperbolic semblance velocity scans for LASE CDP gathers near the shelf edge. The array velocity for the reflection from the top of the carbonate sequence at 4.2 seconds of traveltime is better resolved in the 0-10 km scan, but the array velocities from the shallow part of the section are best defined from the 0-4 km velocity scan.

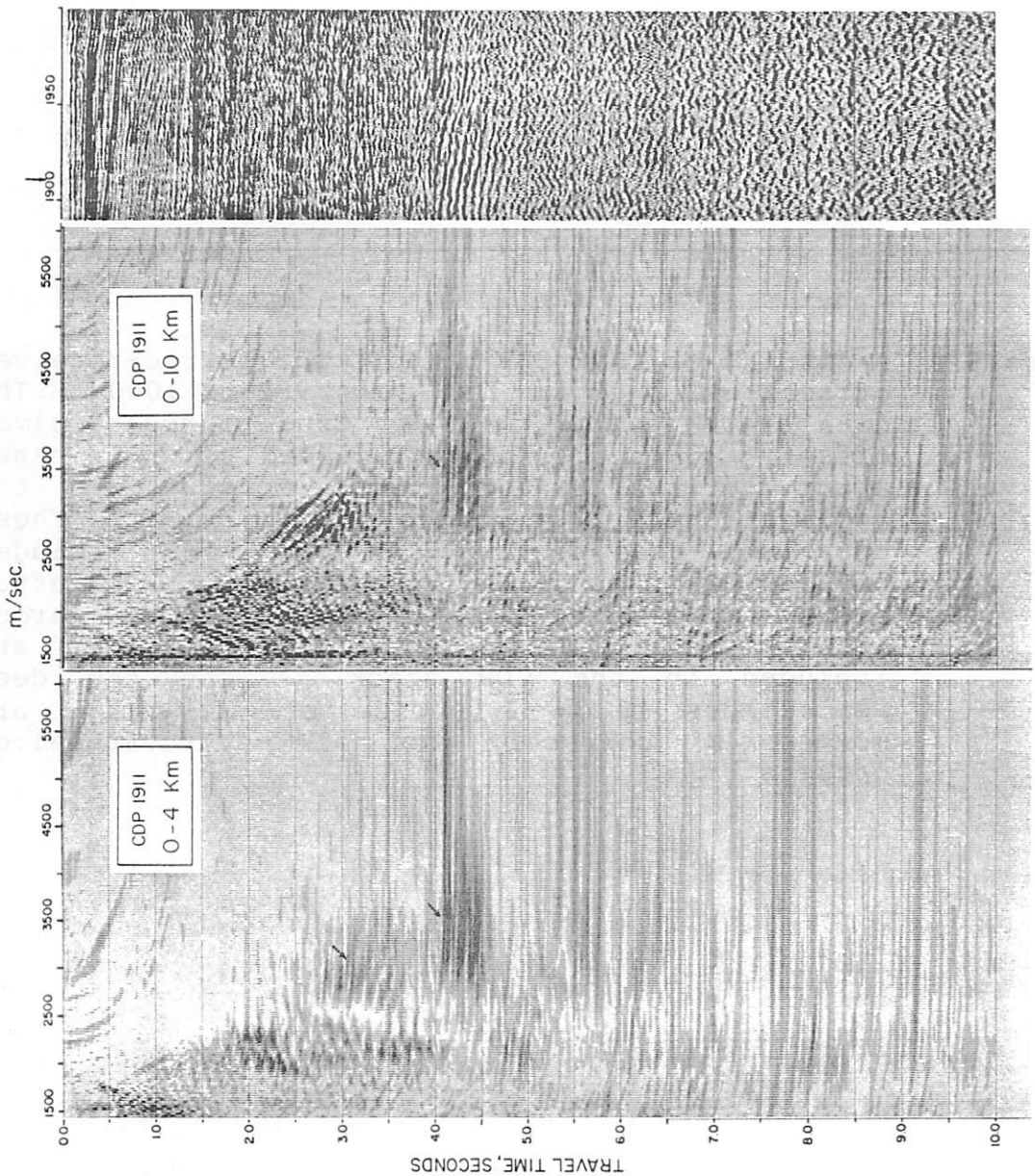
CDP 1911
0 - 4 Km
CDP 1911
0 - 10 Km
m/sec
1500
2500
3500
4500
5500
1900
1950
0.0
1.0
2.0
3.0
4.0
5.0
6.0
7.0
8.0
9.0
10.0
TRAVEL TIME, SECONDS

FIGURE 5

Figure 6 A display of LASE CDP gathers for source-receiver offsets of 0-10 km for CDPs 982 to 1000. The data are displayed at their true source-receiver offset with three CDPs displayed in each panel after correcting for normal moveout and the application of post-normal moveout mutes. These data were used in the CDP stack which includes offsets of 0 to 10 km. In this region, after about 4.5 seconds of two-way time, the larger offsets from the synthetic LASE aperture are included in the CDP stack. Note the deep reflections below 6 seconds of traveltime are moved out correctly for all source-receiver offsets.

XT) MUTES applied to moved out LASE gathers

FIGURE 6

Figure 7 LASE Line 6 stacked record section with the velocity functions derived from the ESPs superimposed. Below about 4.5 seconds of two-way normal time source-receiver offsets of 0-10 km are included in the stack. A 750 msec AGC and time-varying bandpass filter were applied to enhance the deep reflection events. The stacked data were also mixed by a factor of 9 and spatially decimated by a factor of 3 to further increase the signal to noise level at depth. The effect of the water column has also been removed so that the reflectors beyond the shelf edge better approximate their true position.

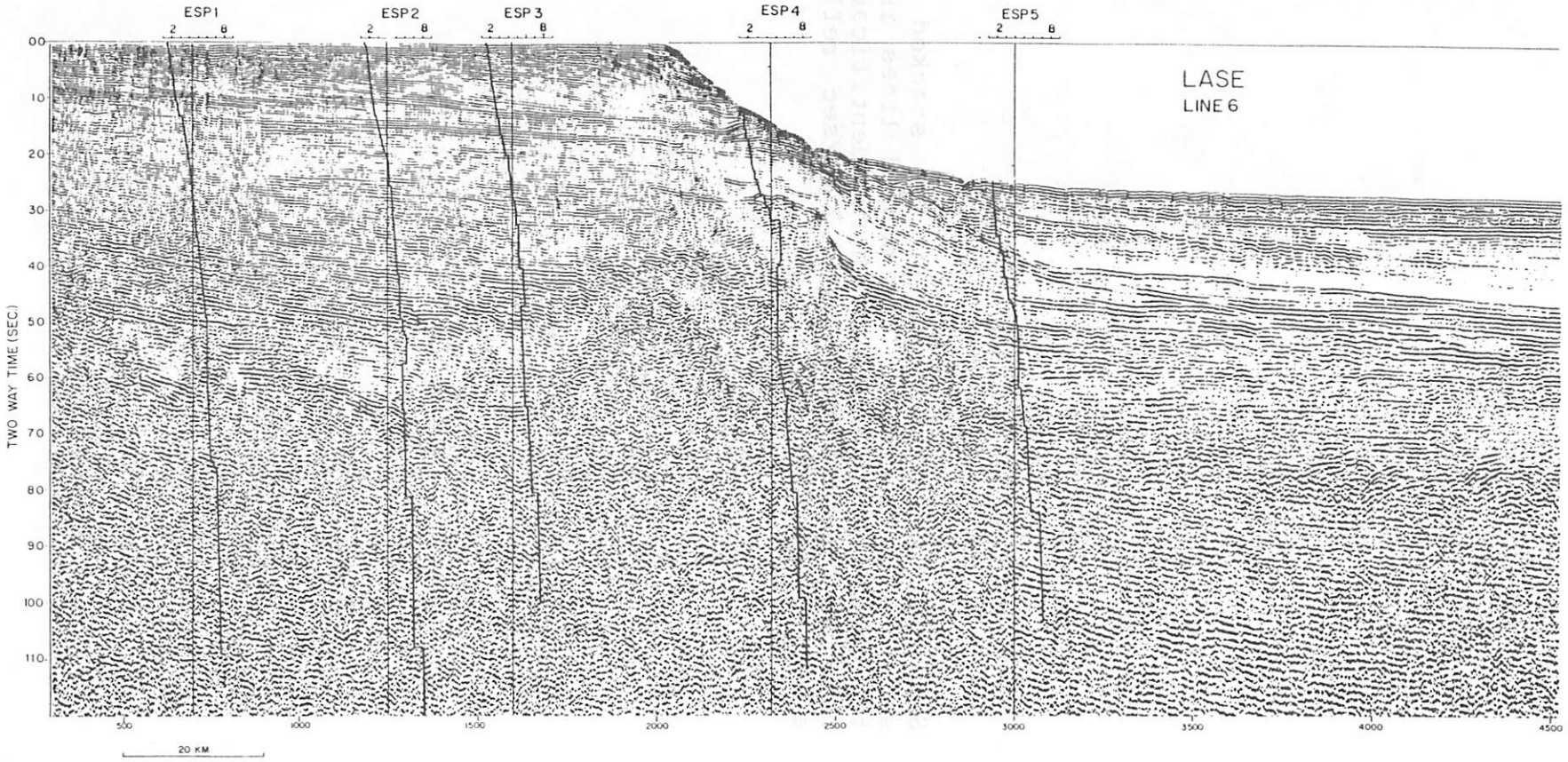
ESP1
ESP2
ESP3
ESP4
ESP5
2
8
LASE
LINE 6
TWO WAY TIME (SEC.)
00
10
20
30
40
50
60
70
80
90
100
110
500
1000
1500
2000
2500
3000
3500
4000
4500
20 KM

FIGURE 7

Figure 8 Schematic interpretation of the stacked record section of Figure 7. The dashed lines indicate the area between the ESPs where identification of oceanic basement and the 7.2 km/sec reflection event became difficult.

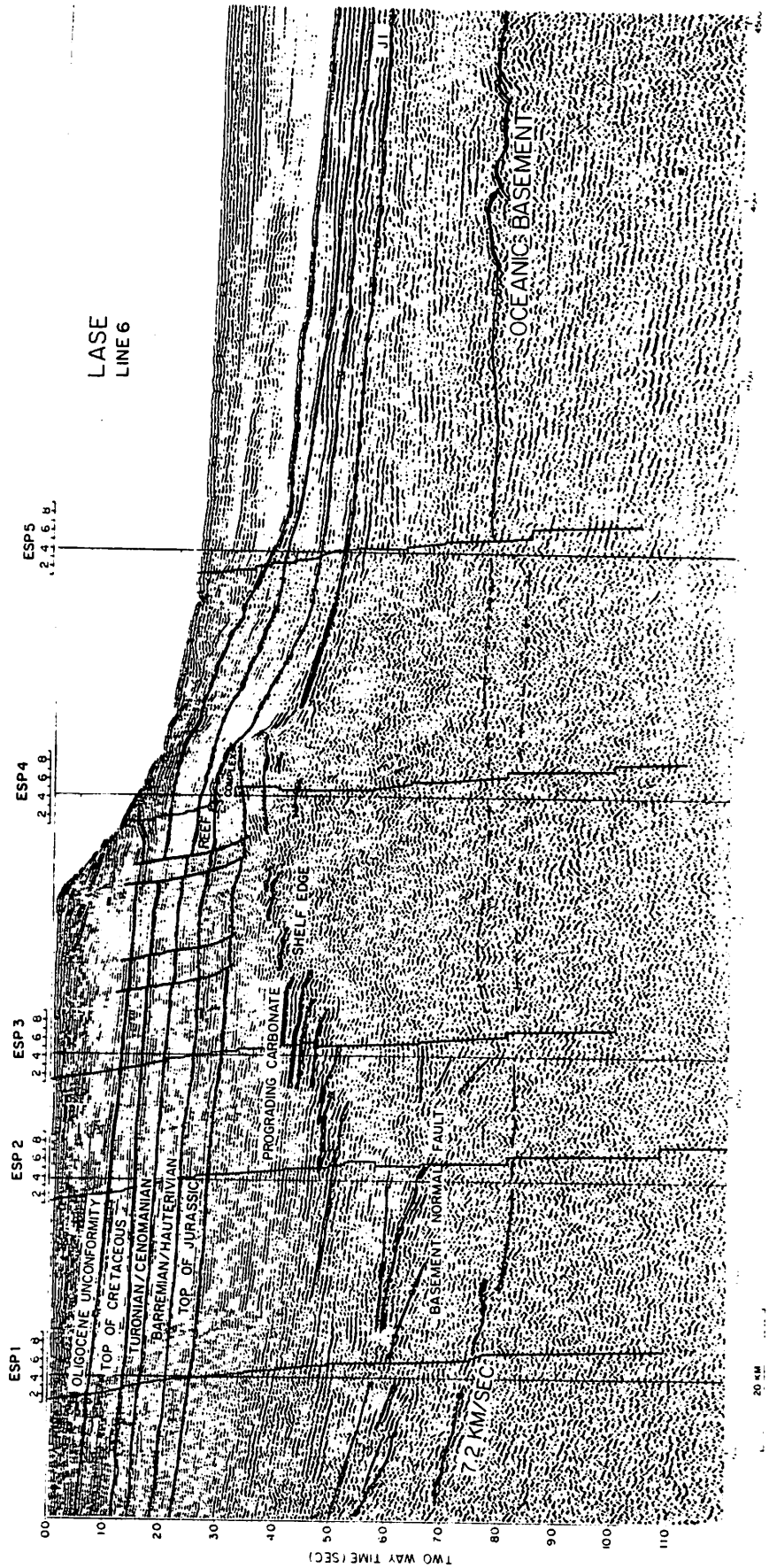
LASE
LINE 6
ESP1
ESP2
ESP3
ESP4
ESP5
OLIGOCENE UNCONFORMITY
TOP OF CRETACEOUS
TURONIAN/CENOMANIAN
BARREMIAN/HAUTERIVIAN
TOP OF JURASSIC
REEF
PROGRADING CARBONATE
SHELF EDGE
BASEMENT NORMAL FAULT
7.2 KM/SEC
OCEANIC BASEMENT
TWO WAY TIME (SEC)
00
10
20
30
40
50
60
70
80
90
100
110

FIGURE 8

Figure 9 Comparison of the 0-4 km CDP stacked record section (upper) and 0-10 km CDP stacked record section (lower) from the Outer Carbonate Bank area. The improved multiple attenuation in the 0-10 km stack makes it possible to trace the reflectors under the reef complex landward.

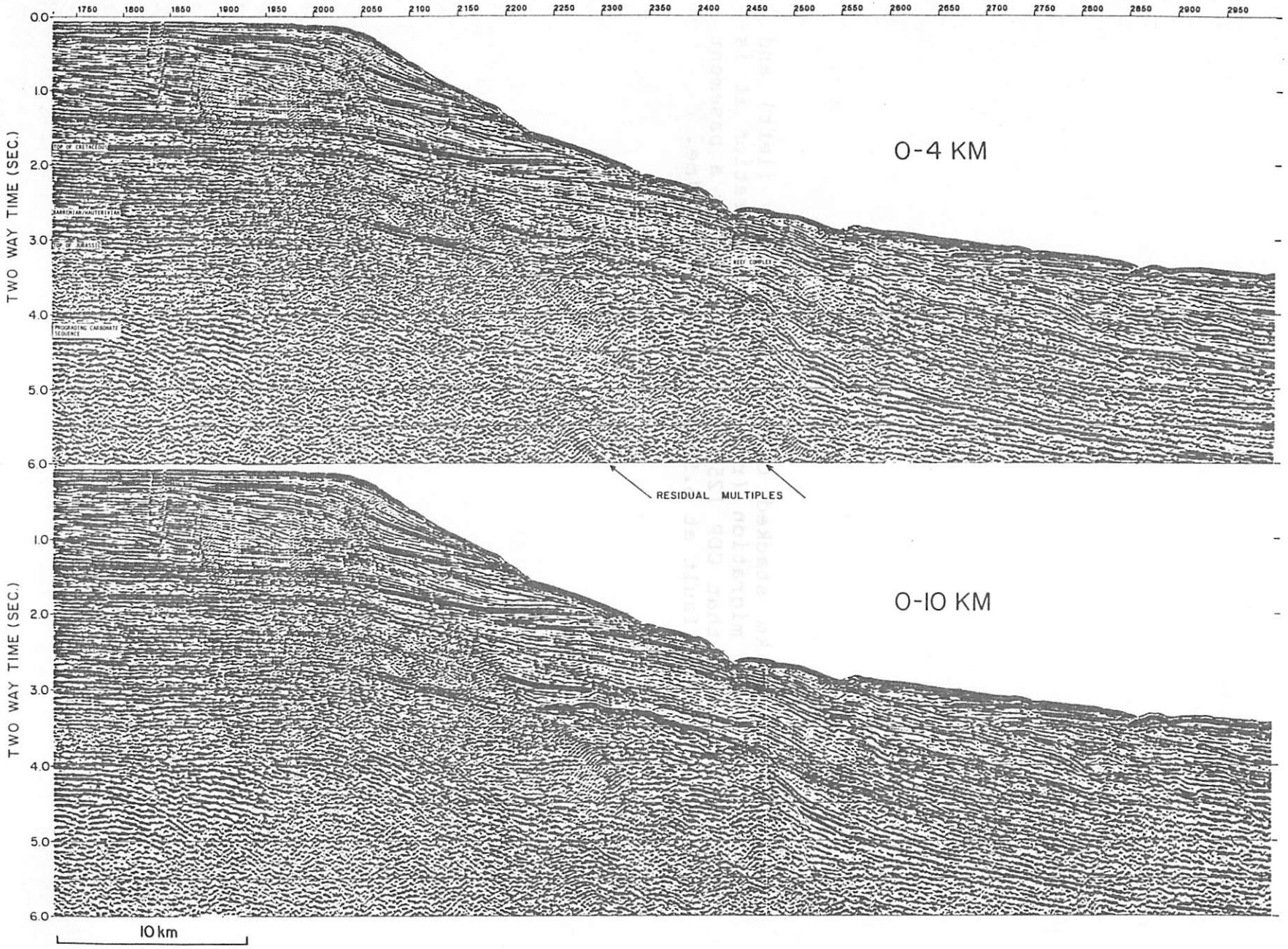
1750 1800 1850 1900 1950 2000 2050 2100 2150 2200 2250 2300 2350 2400 2450 2500 2550 2600 2650 2700 2750 2800 2850 2900 2950
TWO WAY TIME (SEC.)
0.0
1.0
2.0
3.0
4.0
5.0
6.0
TOP OF CRETACEOUS
BARREMIAN/HAUTERIVIAN
TOP OF JURASSIC
PROGRADING CARBONATE SEQUENCE
REEF COMPLEX
0-4 KM
RESIDUAL MULTIPLES
TWO WAY TIME (SEC.)
0.0
1.0
2.0
3.0
4.0
5.0
6.0
0-10 KM
10 km

FIGURE 9

Figure 10 0-10 km stacked CDP record section (left) and after migration (right). After migration it is clear that CDP 1250 marks the edge of a basement normal fault at 6.5 seconds of traveltime.

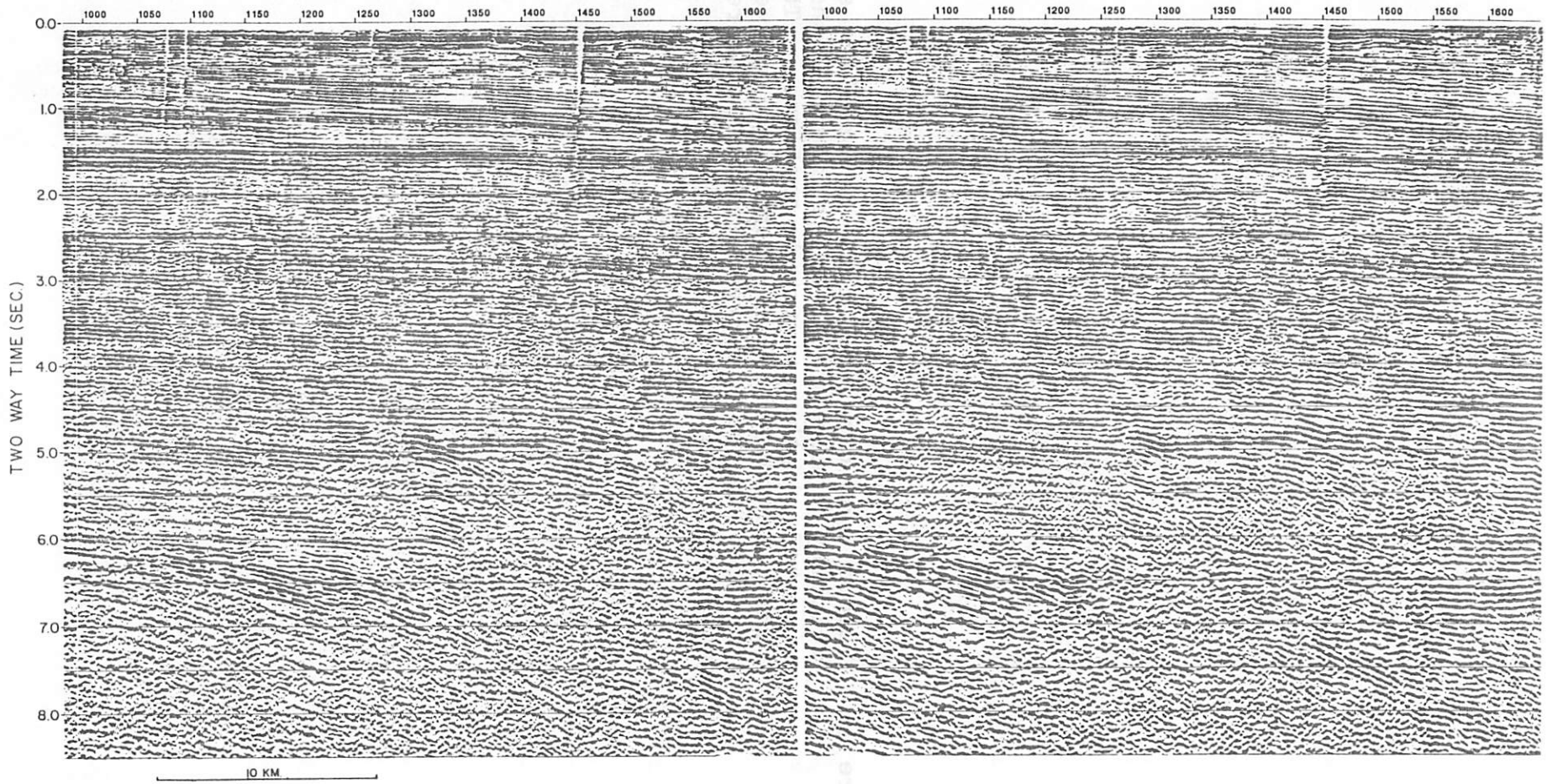
LASE
LINE 6
1000
1050
1100
1150
1200
1250
1300
1350
1400
1450
1500
1550
1600
0.0
1.0
2.0
3.0
4.0
5.0
6.0
7.0
8.0
TWO WAY TIME (SEC.)
10 KM.

FIGURE 10

Figure 11 Velocities obtained from hyperbolic semblance velocity analysis and Dix's formula shown on a migrated depth converted section. The major reflection events were identified and velocities for the intervals between reflectors were derived wherever possible.

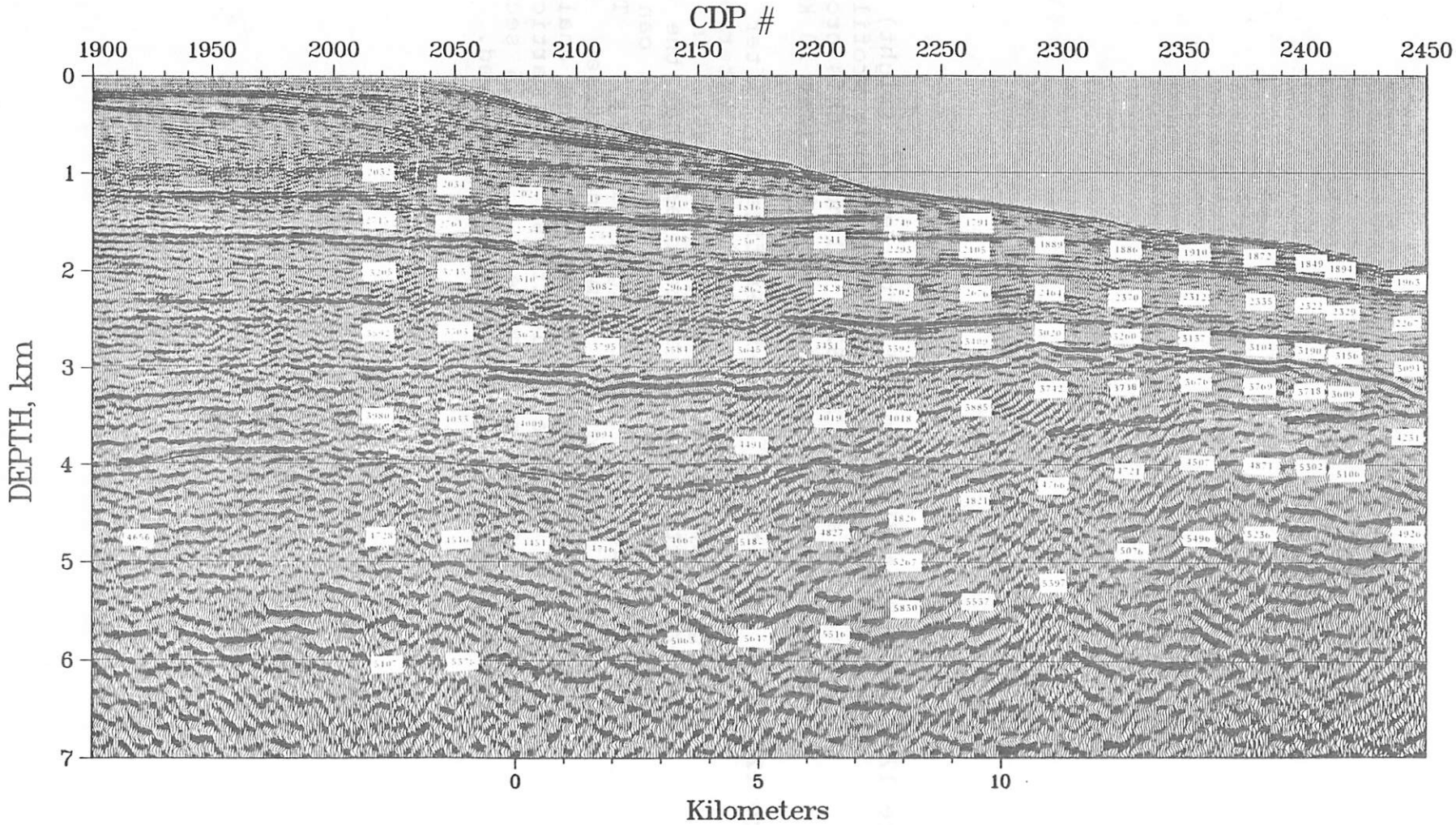
CDP #
1900
1950
2000
2050
2100
2150
2200
2250
2300
2350
2400
2450
DEPTH, km
0
1
2
3
4
5
6
7
0
5
10
Kilometers

FIGURE 11

Figure 12a LASE Expanding Spread Profile 3A (right) and stacked CDP section (left), where this profile is located at about CDP 1620. Although this profile extends to 50 km, we show only the first 20 km.

Figure 12b LASE Expanding Spread Profile 3A, after f-k filtering, designed to eliminate water-borne energy (low phase velocity arrivals). In this record section it is quite clear that the wide angle reflections from 4 to 6.5 seconds can now be followed to the larger offsets. These arrivals' reflection time and offset were digitized and used in T^2-X^2 reflection analysis to derive interval velocities. Of particular interest is the zone between 5 and 6.5 seconds where a velocity of 5.7 km/sec is observed.

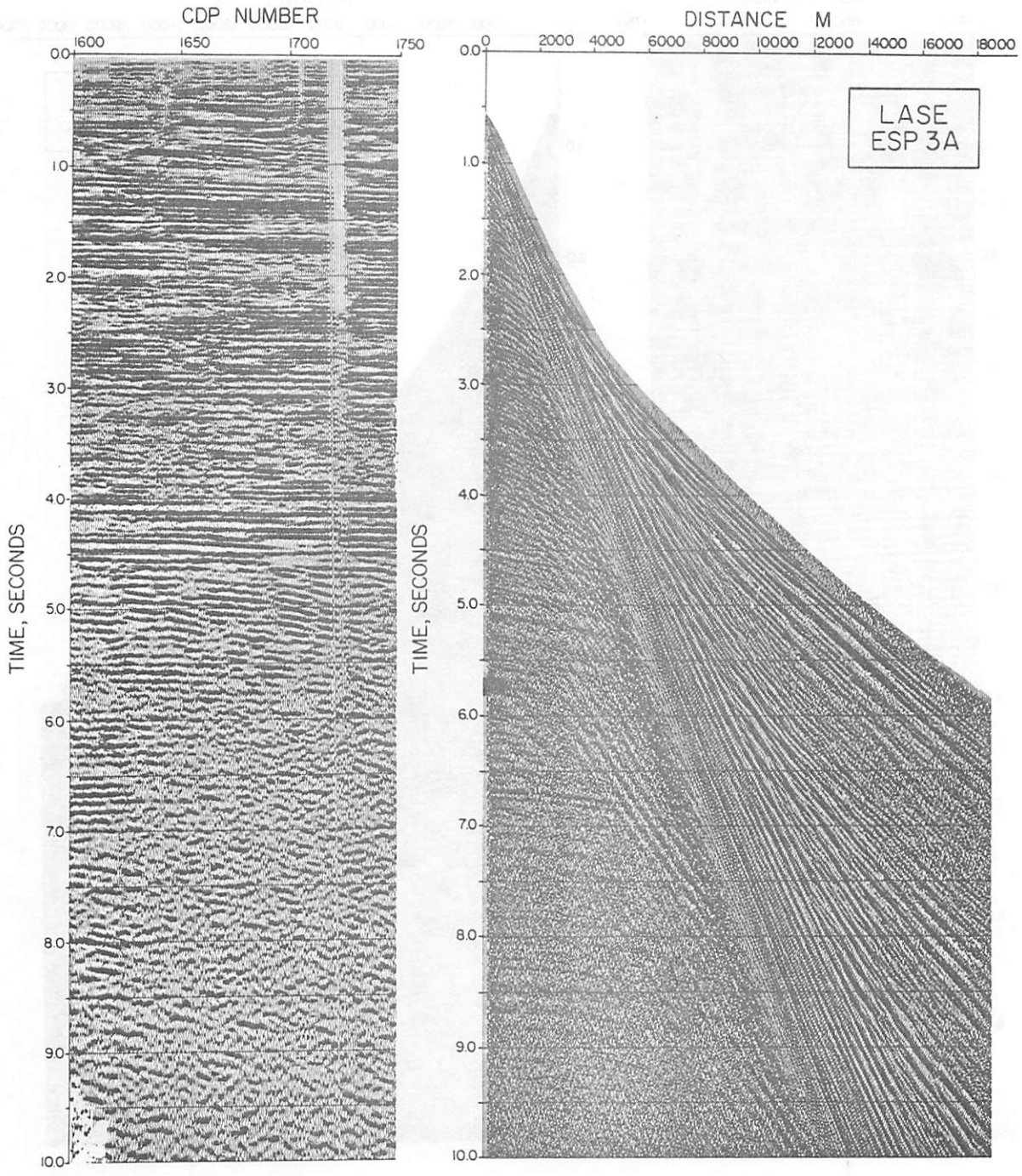
CDP NUMBER
1600
1650
1700
1750
TIME, SECONDS
0.0
1.0
2.0
3.0
4.0
5.0
6.0
7.0
8.0
9.0
10.0
DISTANCE M
0
2000
4000
6000
8000
10000
12000
14000
16000
18000
LASE
ESP 3A

FIGURE 12a

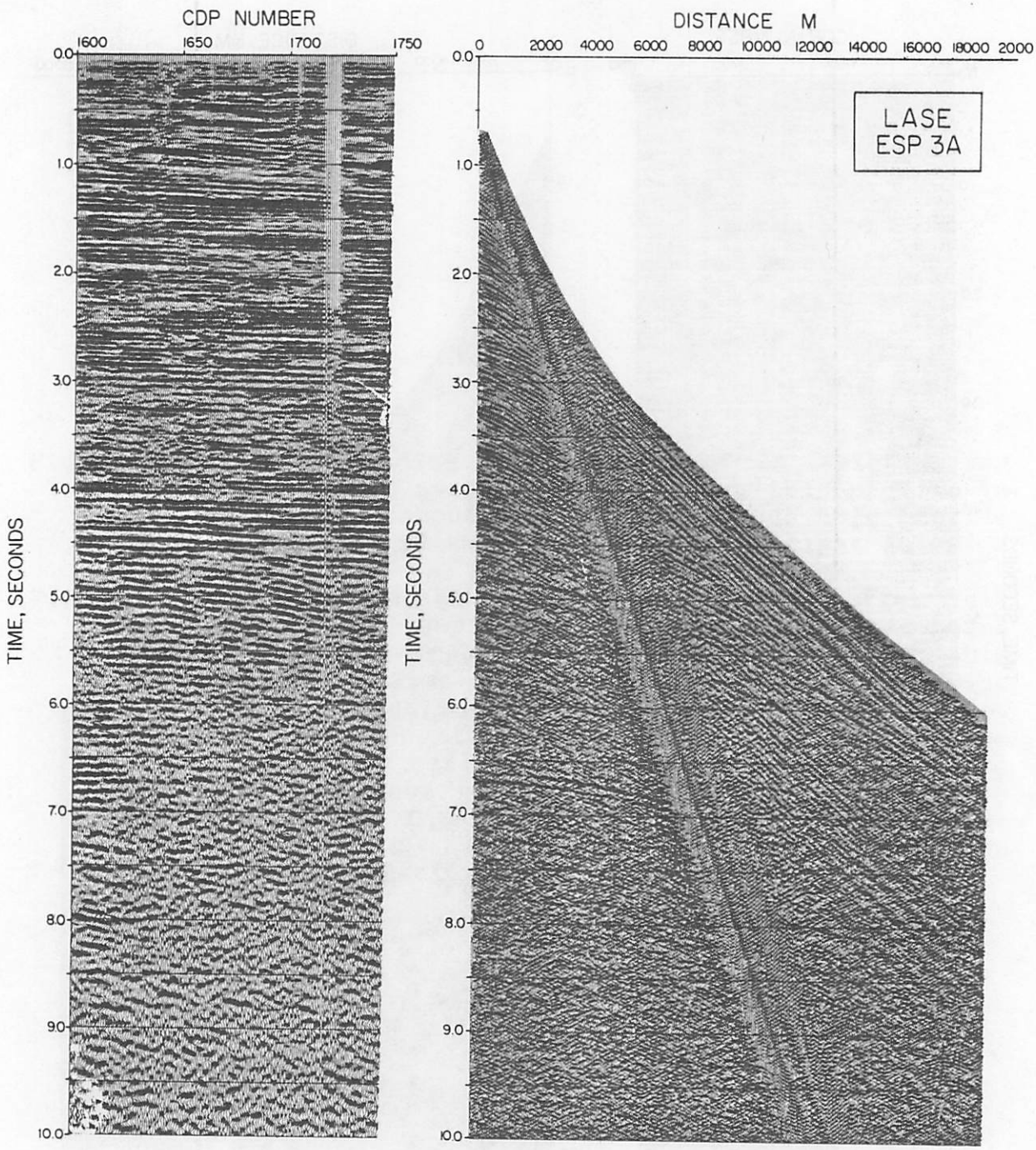
CDP NUMBER
1600
1650
1700
1750
TIME, SECONDS
0.0
1.0
2.0
3.0
4.0
5.0
6.0
7.0
8.0
9.0
10.0
DISTANCE M
0
2000
4000
6000
8000
10000
12000
14000
16000
18000
2000
LASE
ESP 3A

FIGURE 12b

Figure 13 Comparison of the velocity results and methods used in deriving the final solution for ESP 3 and 3A. Interval velocities are shown on the left in terms of traveltime and on the right in terms of depth. The bars on the time section show the limits of the various methods. Since the tau-p method yields the most detail, these results were used for the upper part of the section, after modification to ensure matching of reflections seen in the T-X data (Figures 14a, 14b). The T^2-X^2 velocities fit quite well, except that they provide no resolution in the shallow part of the section. The closely packed curves reaching down to 2 seconds in time and 3 km in depth are from first arrival analyses from four nearby LASE CDP gathers. (We include these curves here to show how well the results agree.) In the high velocity - low velocity sequence between 4 and 6.5 seconds, the T^2-X^2 results are the "Layercake" model, while the ESP 3 T-X results contain gradients. The principal value of the T^2-X^2 results was in confirming the velocities of the high velocity - low velocity sequence.

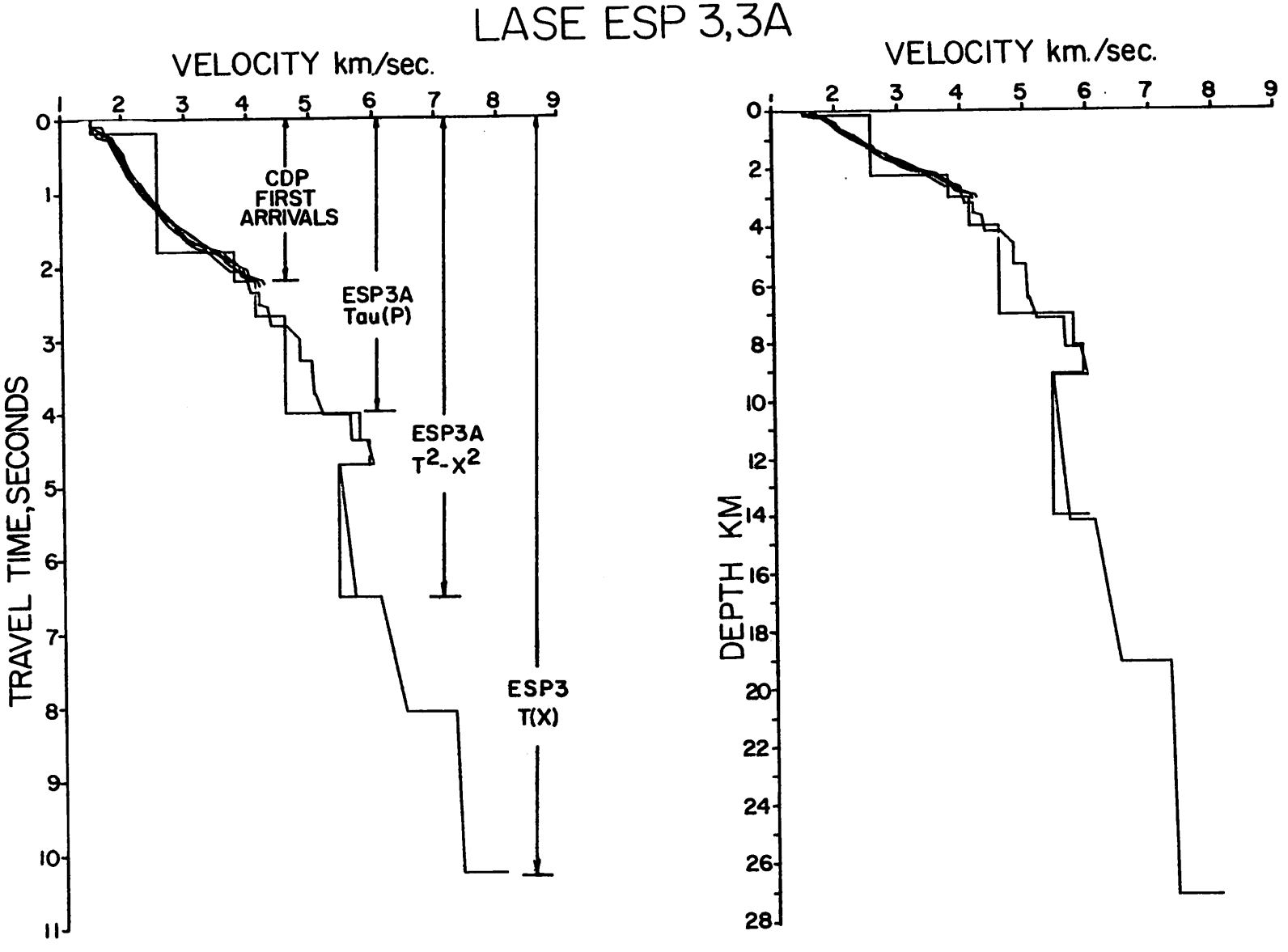
LASE ESP 3,3A
VELOCITY km/sec.
TRAVEL TIME, SECONDS
CDP FIRST ARRIVALS
ESP3A Tau(P)
ESP3A T²-X²
ESP3 T(X)
VELOCITY km./sec.
DEPTH KM

FIGURE 13

Figure 14a As a check on the velocity depth profile derived from ESP 3A, the interval velocities were converted to stacking velocities for offsets of 0 to 20 km and the data corrected for normal moveout. The reflection trajectories are now approximately horizontal, indicating that the stacking velocities, derived from interval velocities are correct.

Figure 14b A detail of the reflection at 6.5 seconds two-way time at the base of the low velocity zone. On the left the data were corrected for normal moveout with stacking velocities derived from our final velocity function (Figure 15). It is apparent that this deep event, as indicated by the arrows, follows an approximately horizontal trajectory. To test the presence of the low velocity zone, the data were corrected for normal moveout with the same velocity as the layer above. As shown on the right, it is quite clear that this correction is incorrect for the event at 6.5 sec. Since this event is now undercorrected, a lower velocity is required to make the reflection follow a horizontal trajectory. Even on the left, a slightly lower velocity is implied.

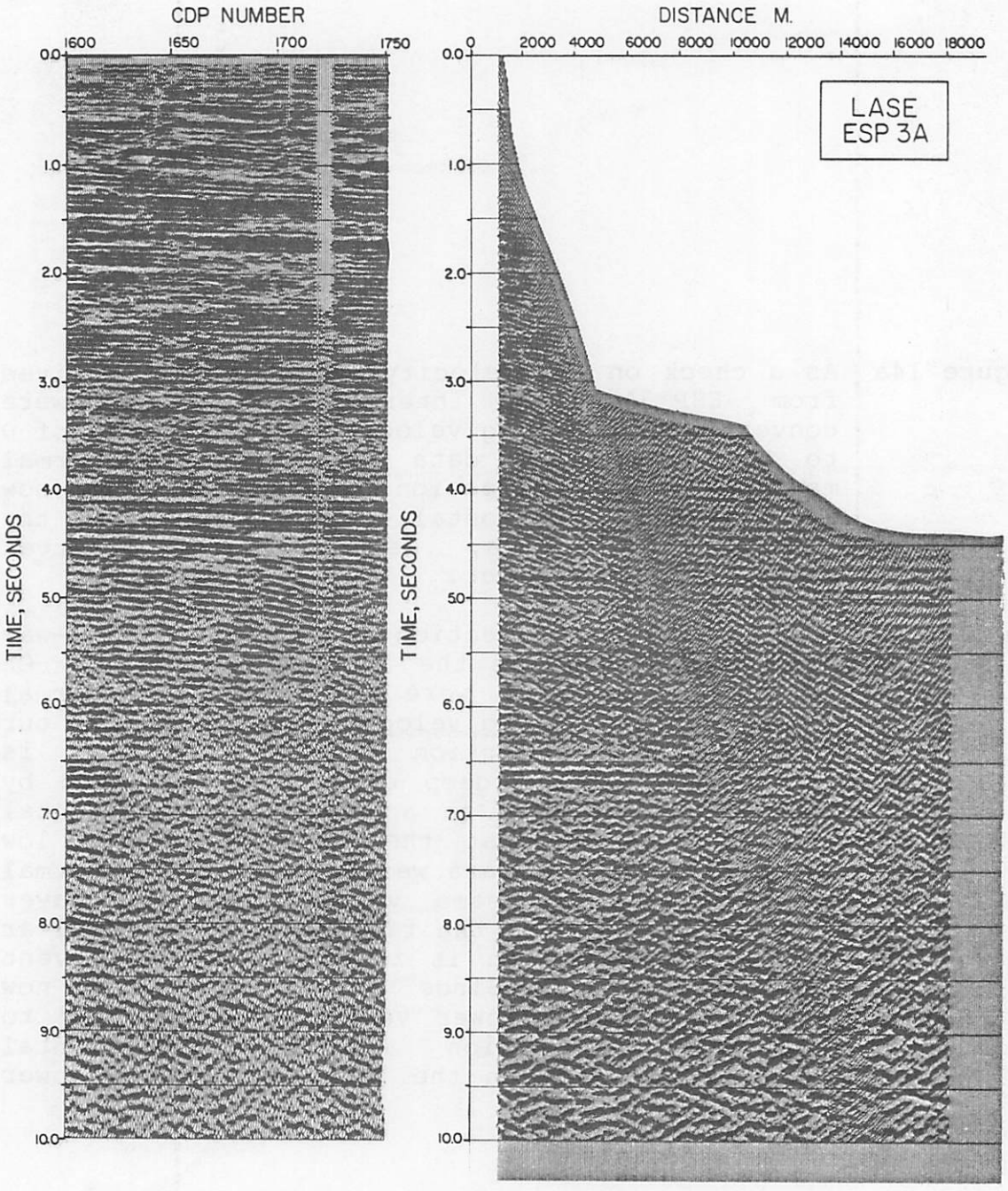
CDP NUMBER
1600
1650
1700
1750
TIME, SECONDS
0.0
1.0
2.0
3.0
4.0
5.0
6.0
7.0
8.0
9.0
10.0
DISTANCE M.
0
2000
4000
6000
8000
10000
12000
14000
16000
18000
LASE
ESP 3A

FIGURE 14a

LASE ESP 3A NMO

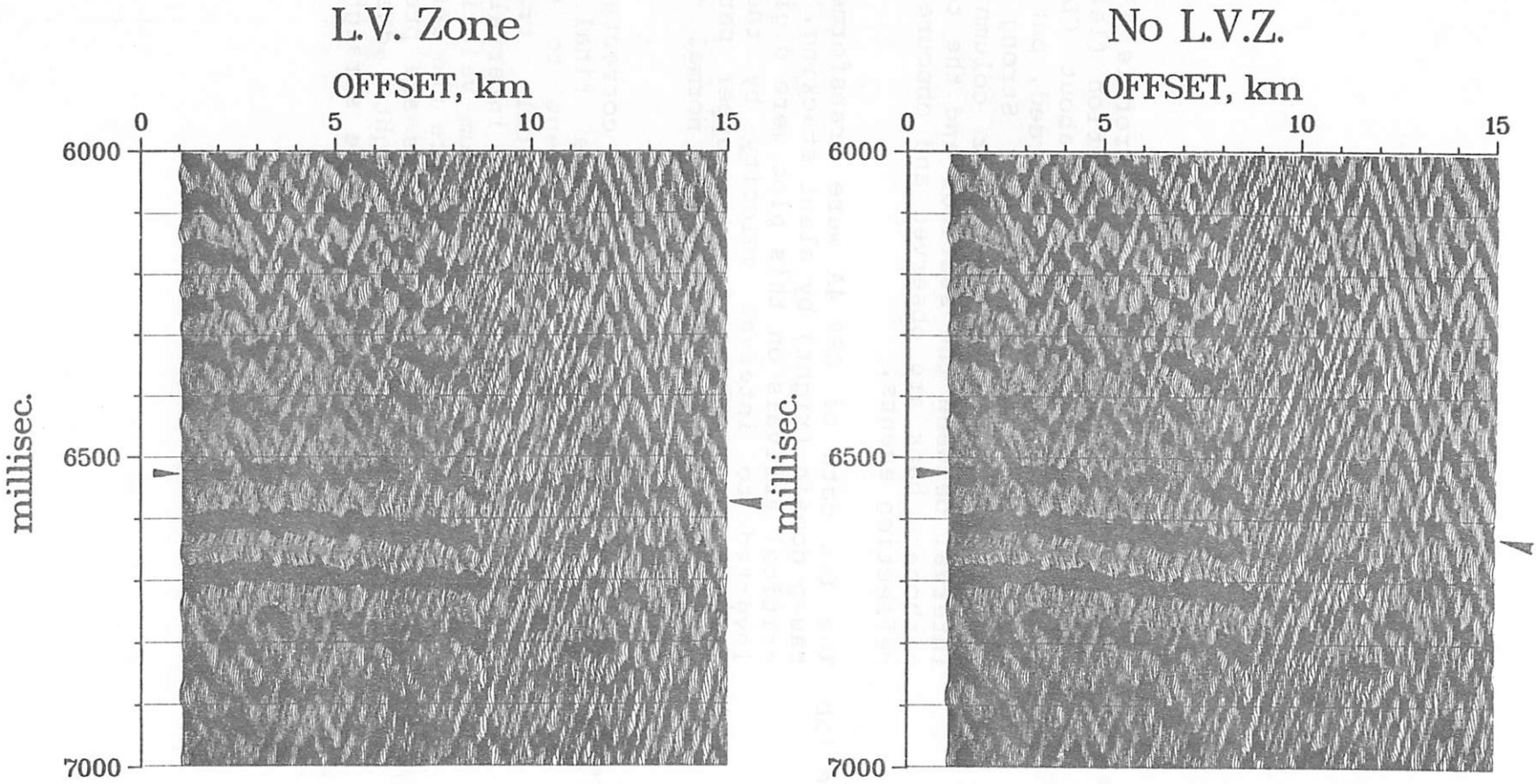

FIGURE 14b

Figure 15a LASE airgun Expanding Spread Profile 4A (right) and the CDP stacked record section (left) where this profile is located at about CDP number 2320. 50 km of data were recorded, but only the first 20 km are displayed. Strong multiple arrivals, both from the water column and the interval between the seafloor and the top of the carbonate bank are observed and obscure any deep reflection events.

Figure 15b The T-X data of ESP 4A were transformed to the tau-p domain (right) by slant stacking. Picks of critical arrivals on this plot were digitized and inverted to interval velocity by the Tau-Sum method. Velocities for the upper part of the section (0-4 sec) of two-way normal time were thus obtained.

Figure 15c The tau-p data of Figure 15b, corrected to two-way normal time, using the final interval velocity function. The extent to which the reflections follow horizontal trajectories reflects the accuracy of the interval velocity function. The original Tau-Sum velocities were iteratively corrected to produce the result shown here. When velocity gradients are present, the arrivals along the far right edge of the corrected tau-p data cannot be straightened but connect between layers.

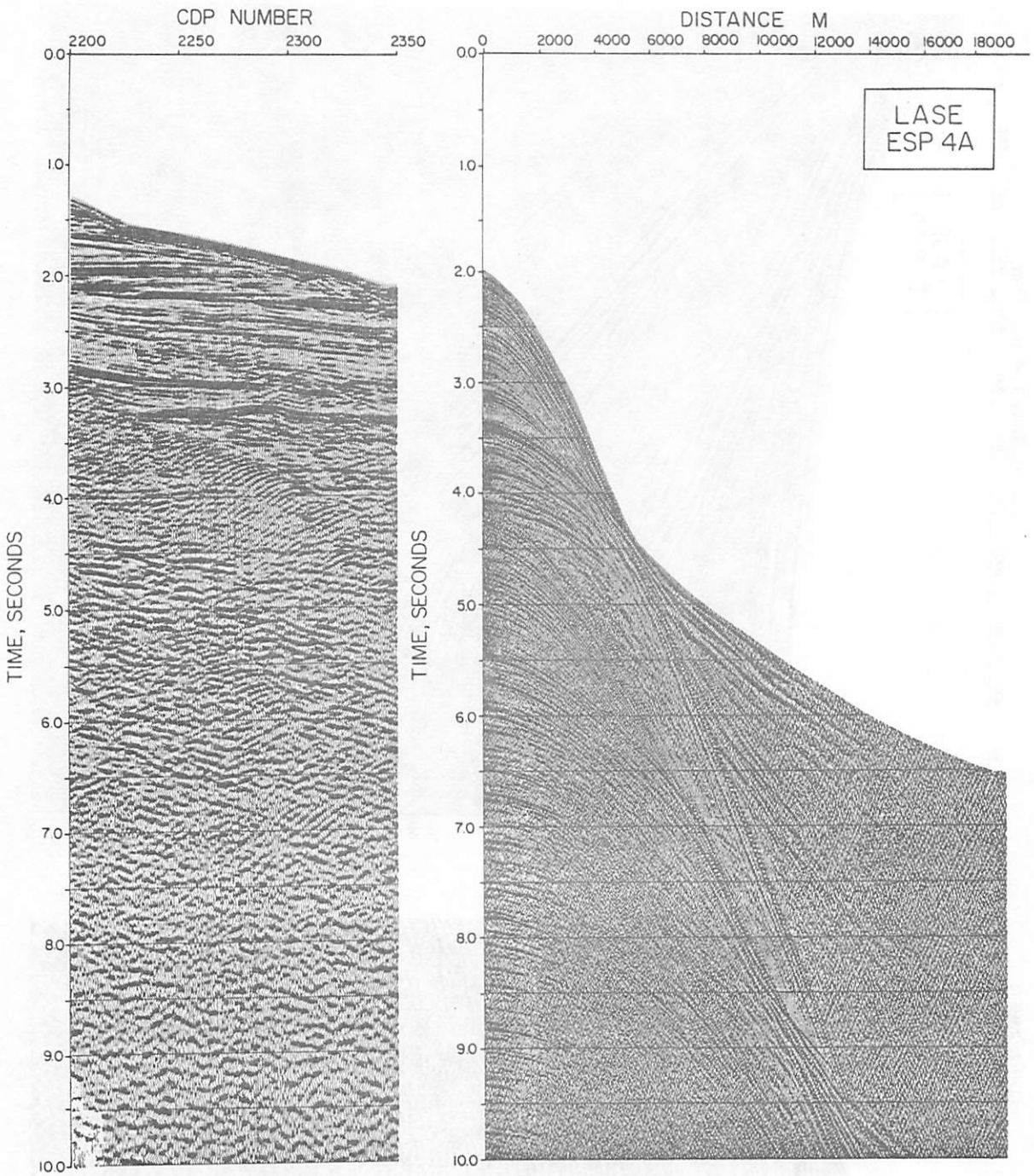
CDP NUMBER
2200
2250
2300
2350
DISTANCE M
0
2000
4000
6000
8000
10000
12000
14000
16000
18000
LASE
ESP 4A
TIME, SECONDS
TIME, SECONDS
0.0
1.0
2.0
3.0
4.0
5.0
6.0
7.0
8.0
9.0
10.0

FIGURE 15a

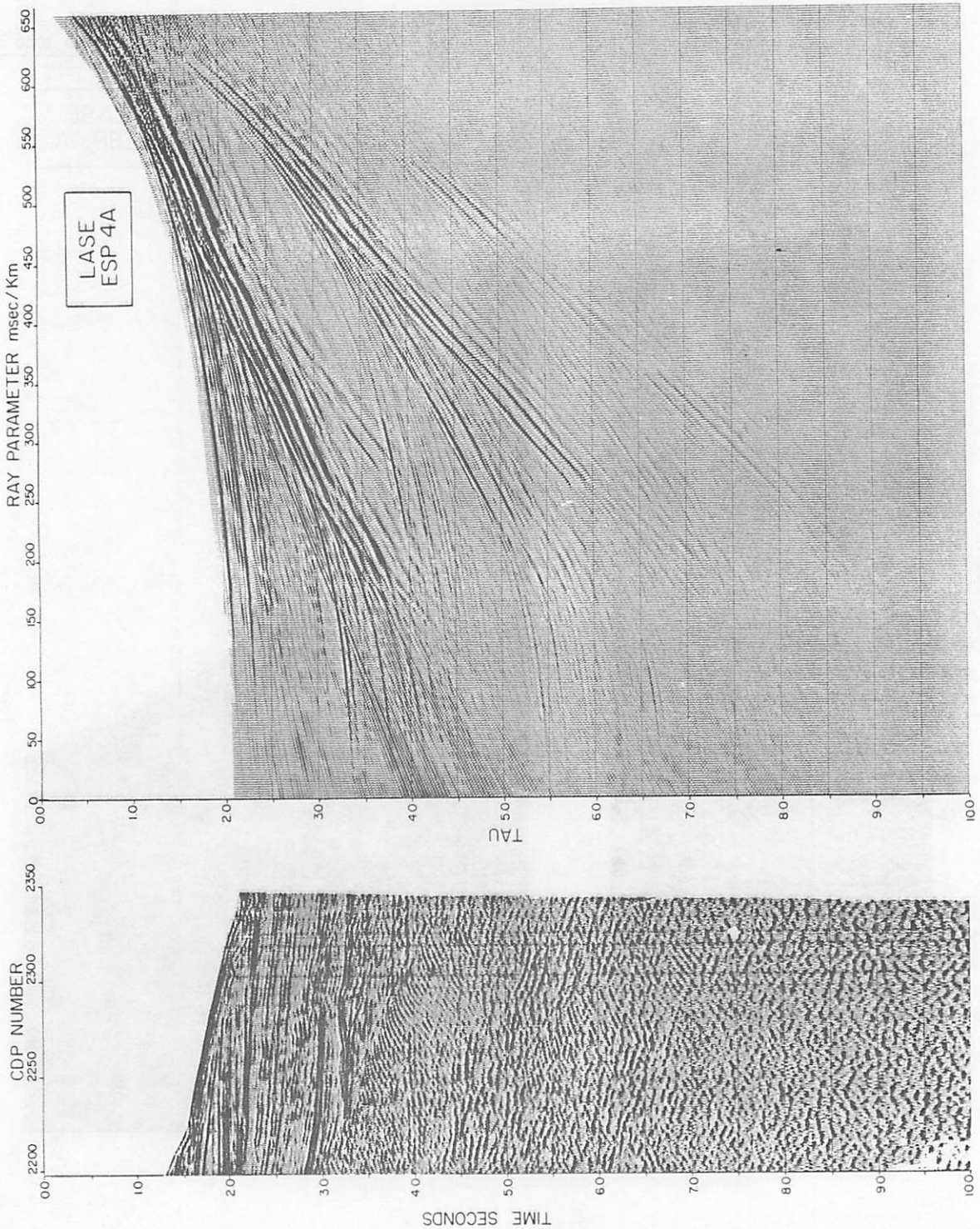
LASE
ESP 4A
RAY PARAMETER msec/Km
0
50
100
150
200
250
300
350
400
450
500
550
600
650
TAU
0.0
10
20
30
40
50
60
70
80
90
100
CDP NUMBER
2200
2250
2300
2350
TIME SECONDS

FIGURE 15b

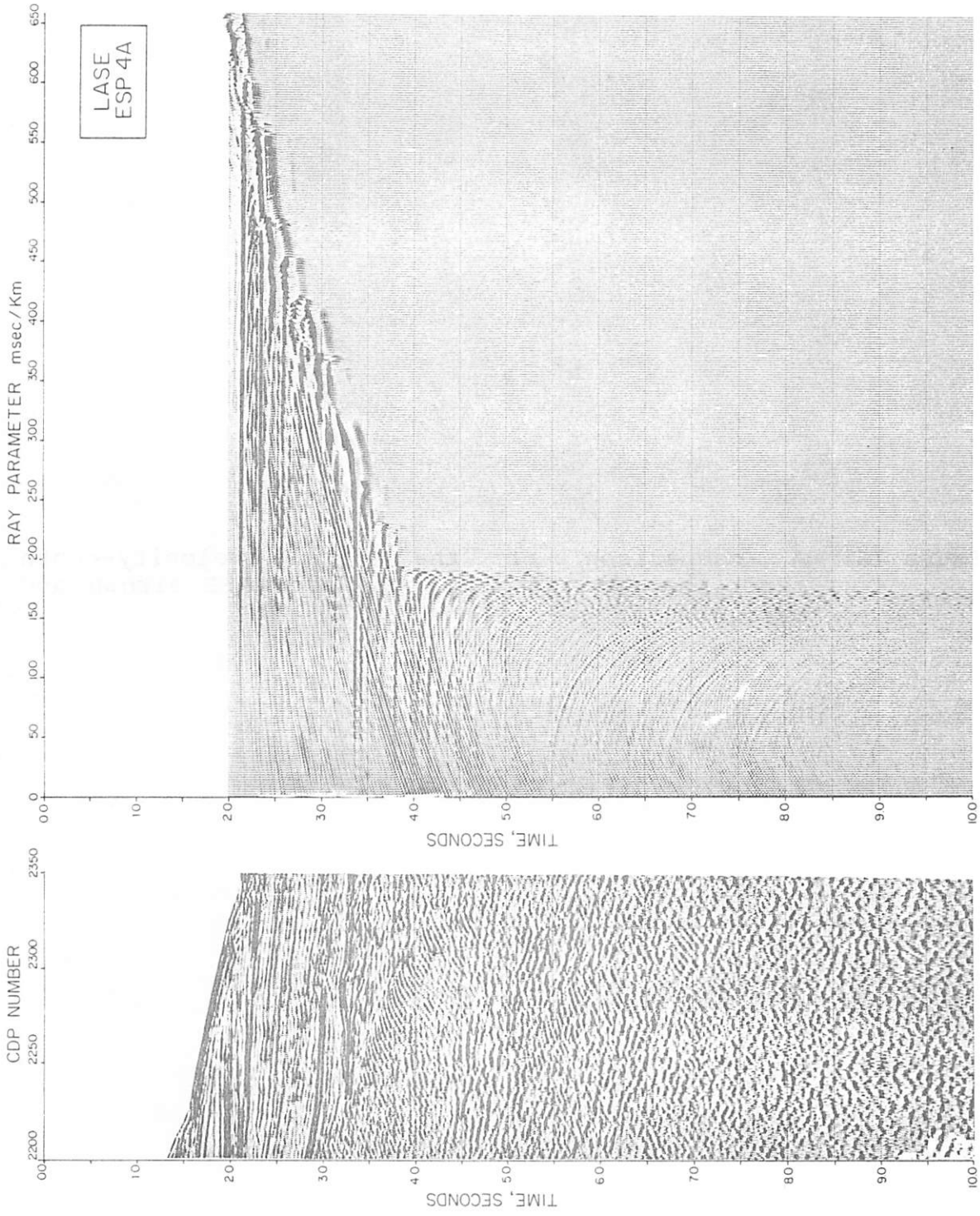
LASE
ESP 4A
RAY PARAMETER msec/Km
0
50
100
150
200
250
300
350
400
450
500
550
600
650
TIME, SECONDS
0.0
10
20
30
40
50
60
70
80
90
100
CDP NUMBER
2200
2250
2300
2350
TIME, SECONDS
0.0
10
20
30
40
50
60
70
80
90
100

FIGURE 15c

Figure 16 A comparison of the final velocity-depth functions derived from both the LASE airgun and explosive ESPs.

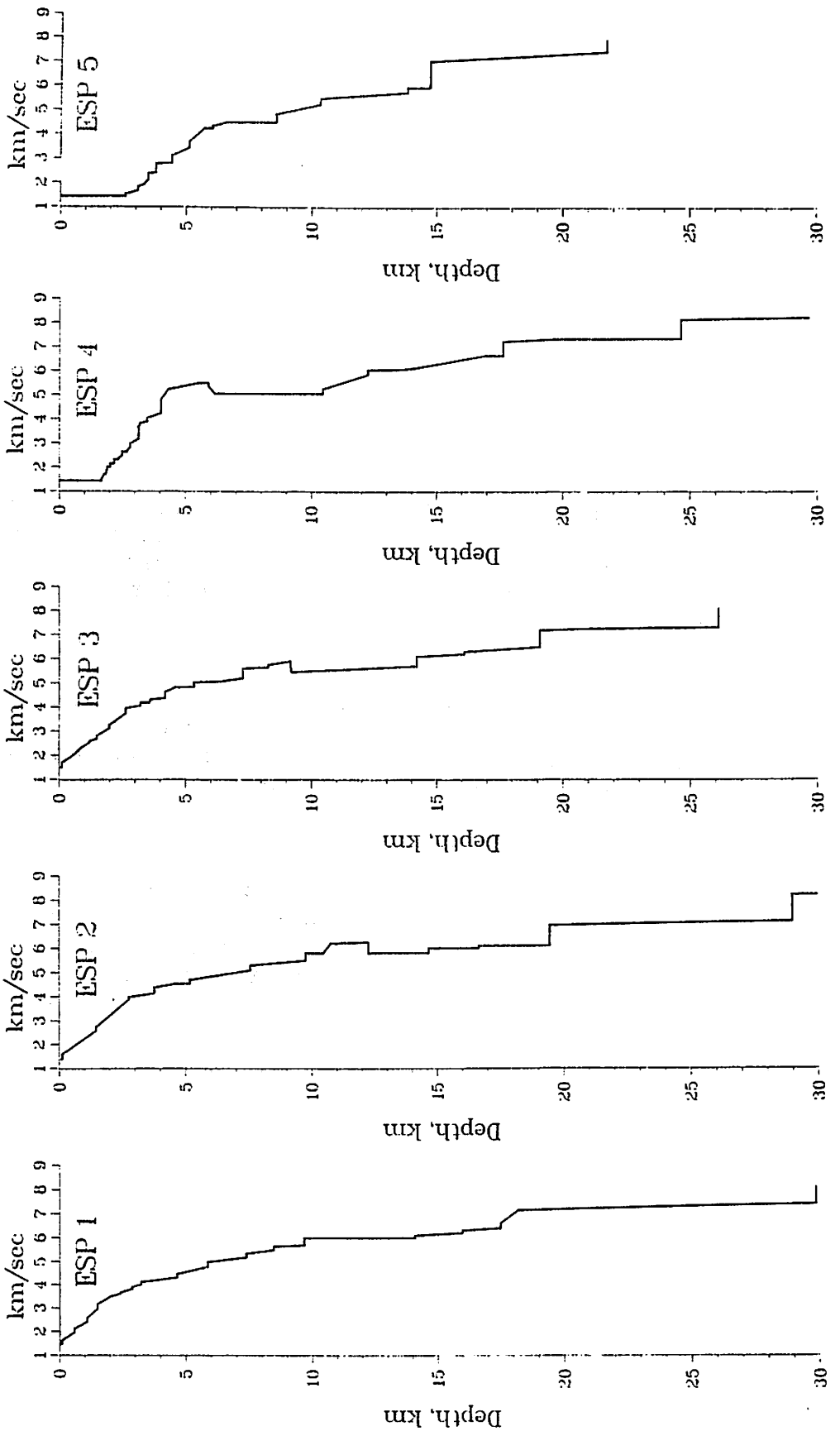
ESP 1
ESP 2
ESP 3
ESP 4
ESP 5
km/sec
Depth, km
0
5
10
15
20
25
30
1 2 3 4 5 6 7 8 9

FIGURE 16

Figure 17a LASE explosive ESP 2 reduced with a velocity of 5.5 km/sec. The traveltimes predicted from the final model (Figure 16) are superimposed and the location of the points of critical reflection are marked by arrows.

Figure 17b LASE explosive ESP 3 reduced with a velocity of 5.5 km/sec. The traveltimes predicted from the final model (Figure 16) are superimposed and the location of the points of critical reflection are marked by arrows.

Figure 17c LASE explosive profile ESP 4 reduced with a velocity of 5.5 km/sec. The traveltimes predicted from the final model (Figure 16) are superimposed and the location of the points of critical reflection are marked by arrows.

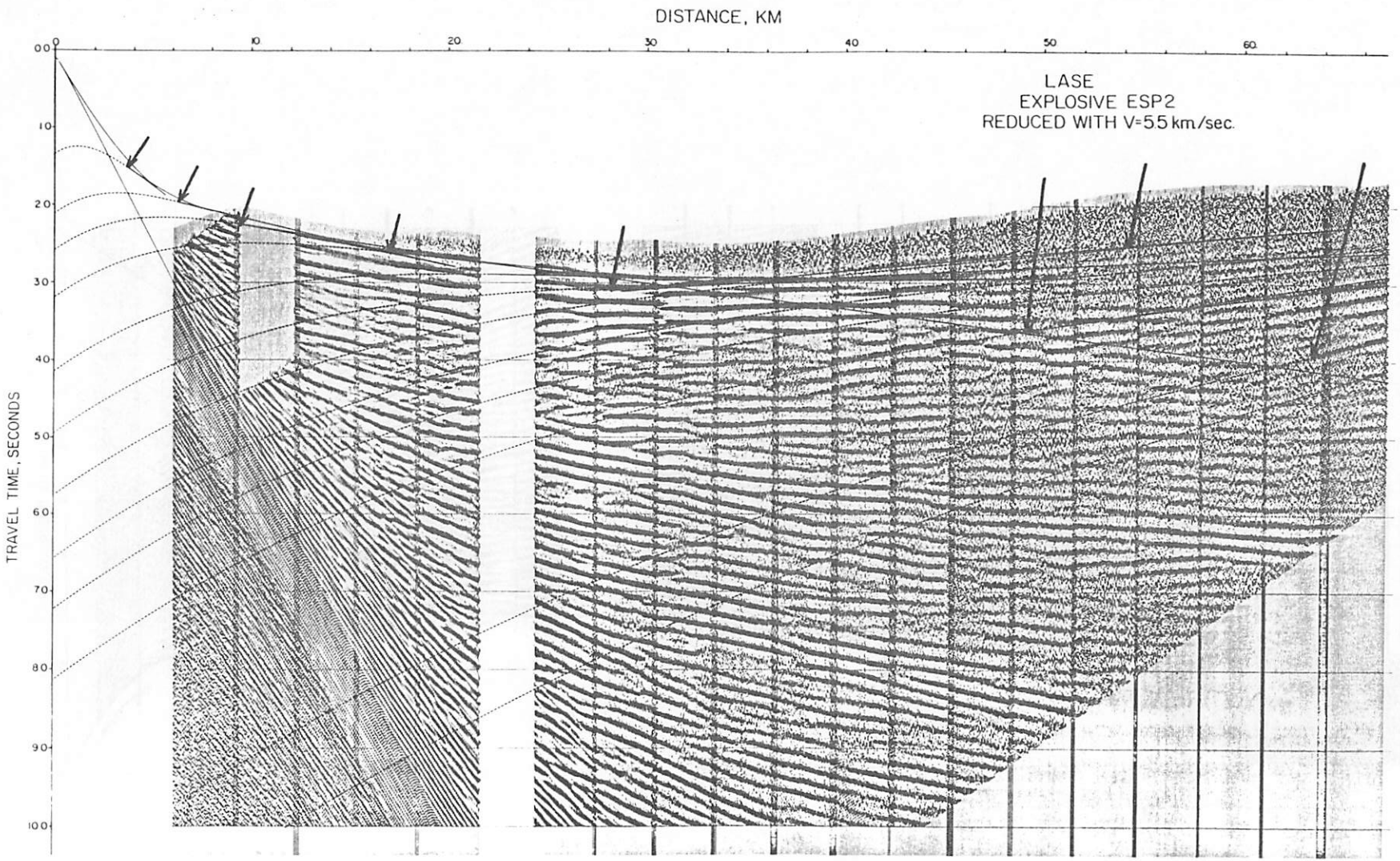
DISTANCE, KM
0
10
20
30
40
50
60
LASE
EXPLOSIVE ESP2
REDUCED WITH V=5.5 km/sec.
TRAVEL TIME, SECONDS
00
10
20
30
40
50
60
70
80
90
100

FIGURE 17a

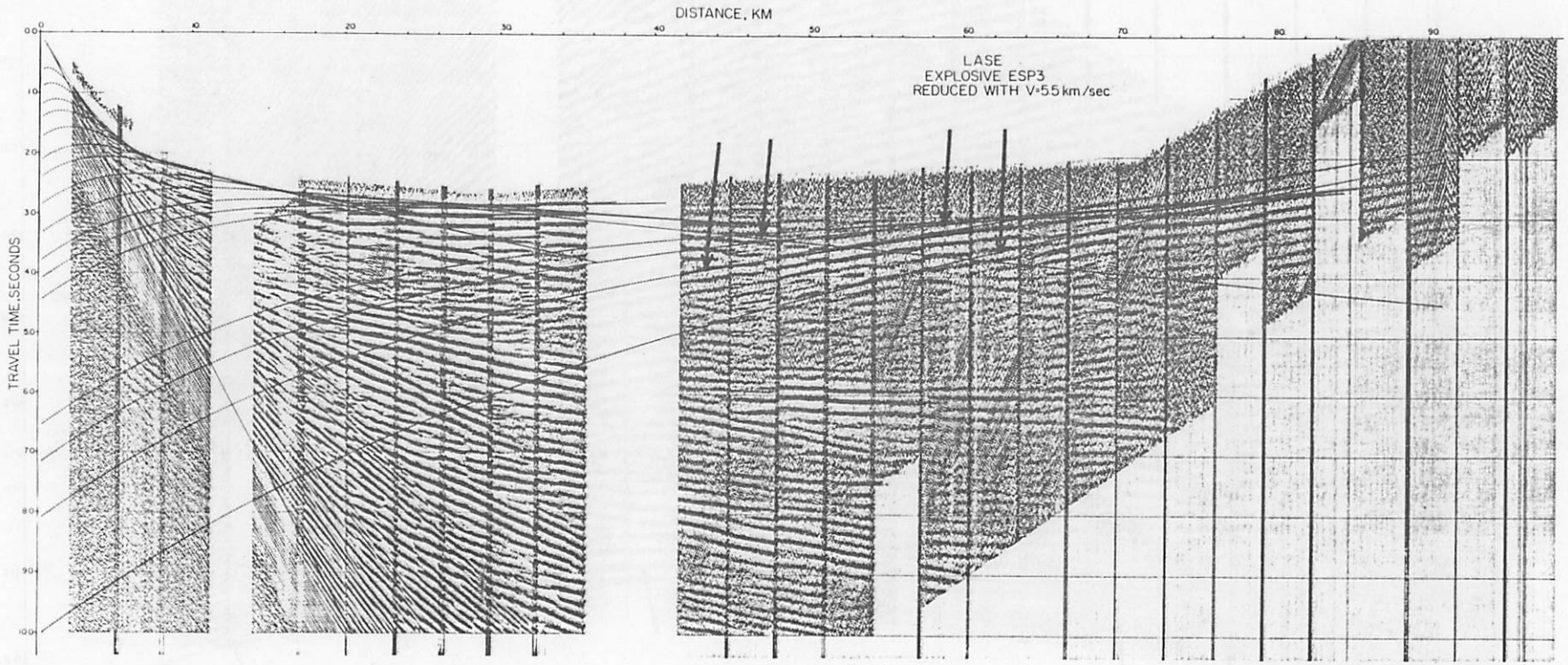
DISTANCE, KM
0
10
20
30
40
50
60
70
80
90
LASE
EXPLOSIVE ESP3
REDUCED WITH V=5.5 km/sec
TRAVEL TIME, SECONDS
00
10
20
30
40
50
60
70
80
90
100

FIGURE 17b

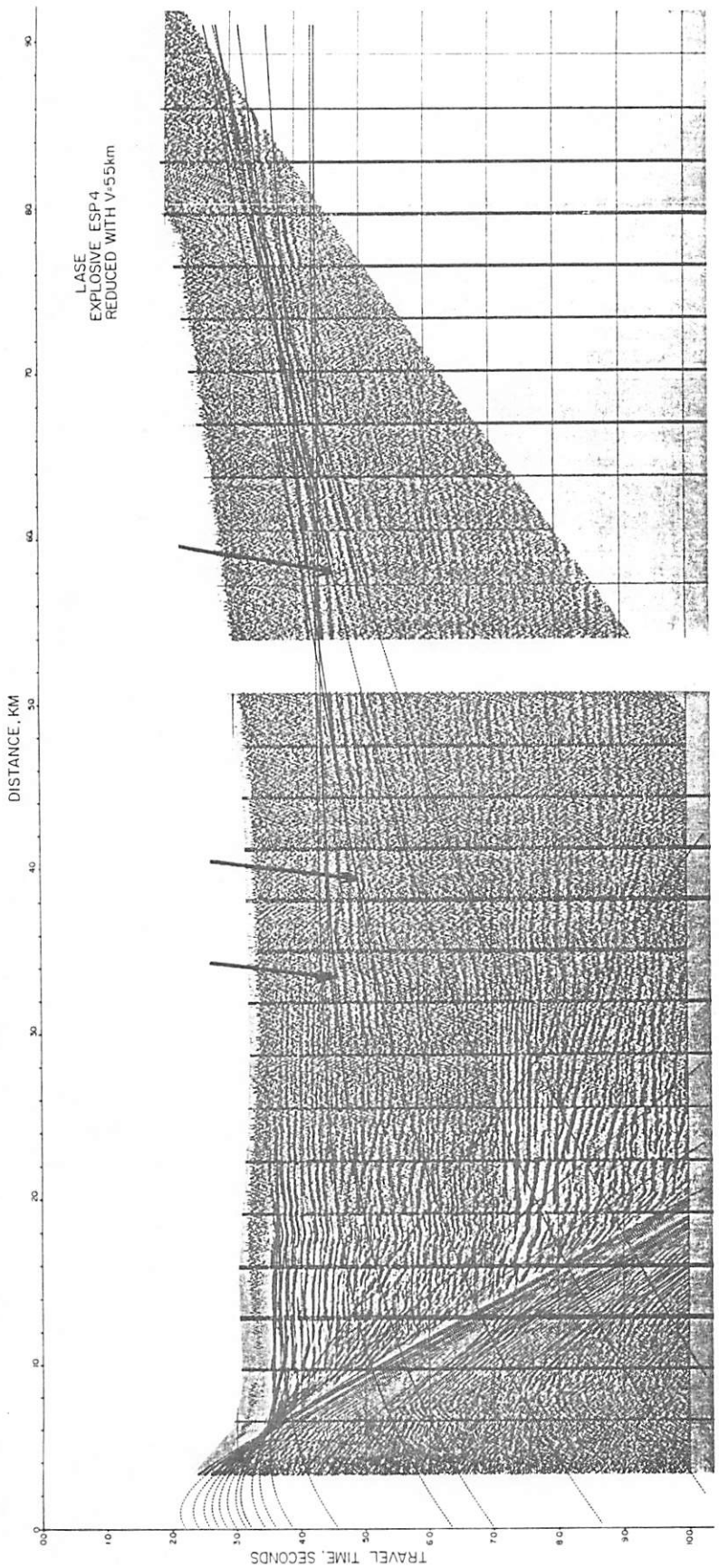
LASE
EXPLOSIVE ESP 4
REDUCED WITH V=5.5km
DISTANCE, KM
TRAVEL TIME, SECONDS

FIGURE 17c